Solid-State Covariance NMR Spectroscopy

AUTHOR(S):

Takeda, Kazuyuki

CITATION:

Takeda, Kazuyuki. Solid-State Covariance NMR Spectroscopy. Annual Reports on NMR Spectroscopy 2015, 84: 77-113

ISSUE DATE:

2015

URL:

http://hdl.handle.net/2433/196666

Solid-state covariance NMR spectroscopy

Kazuyuki Takeda [a,*],

[a] *Division of Chemistry, Graduate School of Science, Kyoto University, 606-8502 Kyoto, Japan*

Abstract

Covariance NMR spectroscopy allows acquisition of spin-spin correlation in a more efficient way compared to the traditional two-dimensional Fourier-transformation NMR spectroscopy, leading to reduction in the experimental time or increase in the sensitivity of the spectrum obtainable within a given experimental time. This article summarizes recent works on covariance NMR, focusing on its applications to solid-state NMR spectroscopy. In addition to a brief survey of the covariance spectroscopy, an open question of whether "inner-product" spectroscopy is more natural is posted. The usefulness of covariance NMR spectroscopy is presented by exploring its applications to solid-state systems of chemical/biological interest. A number of recent reports to further improve its efficiency or to extend the scope of its applicability are reviewed.

Key words: time-saving schemes, covariance

* corresponding author
Email address: takezo@kuchem.kyoto-u.ac.jp (Kazuyuki Takeda).

1 Introduction

In NMR spectroscopy, the sensitivity has been the issues of general interest. The technological/methodological advances in sensitivity enhancement made so far had enabled one to reveal hitherto inaccessible structural information, strengthening NMR spectroscopy as a means for chemical analysis. Further progress in future is anticipated to push NMR spectroscopy, and thereby science, forward. That is why the sensitivity enhanced NMR continues and will continue to be an active research subject matter in the community.

The strategies toward sensitivity enhancement are diverse. One way is to increase nuclear spin polarization, and thereby the macroscopic nuclear magnetization. This can be done straightforwardly either by increasing the static magnetic field or decreasing the sample temperature, so as to raise the equilibrium Boltzmann population difference over the Zeeman levels. Recent remarkable magnet technology realized highly homogeneous fields of up to 23.48 T or above, corresponding to the proton resonance frequency that exceeds 1 GHz. Drastic signal enhancement is possible through nuclear hyperpolarization, which can be realized by dynamic nuclear polarization[1], optical pumping[2], and the Haupt effect[3–8].

The NMR sensitivity can also be enhanced by improving the efficiency of signal detection, instead of, or in combination with, nuclear-spin hyperpolarization. By cooling the NMR sample coil down to cryogenic temperatures, the coil resistance can be reduced. As a result, the Q-factor of the resonance circuit increases, so that higher signal voltages can be extracted from the nuclear spin system. In addition, the thermal noise is expected to be suppressed as

decreasing the temperature, and the overall effect is to enhance the signal-to-noise ratio. Thermal insulation between the coil and the sample was a technical challenge but had been overcome. In practice, it is necessary to cool the preamplifier as well as the sample coil, in order to gain satisfactory enhancement in the sensitivity. Probes incorporating such features are known as cryo probes[9–11], and nowadays commercially available for liquid-state NMR. Cryogenically cooled MRI probes[12,13] and solid-state magic angle spinning (MAS) probes[14–16] have also been reported.

The detection sensitivity can be optimized by employing application-tailored experimental systems. For cases where NMR spectra of two separate spin species need to be measured one after another, an NMR system with parallel receivers[17,18] could improve the throughput of research. When the sample of interest is unconventionally tiny, microcoil probes may be the choice[19–24]. For extremely small samples, force detection can be advantageous over the conventional Faraday detection[25–29].

In addition to such *physical* ways toward sensitivity enhancement, development of acquisition/data-processing methods is also an important trend. The latter has been motivated by the necessity of extracting information of chemical interest within a limited experimental time, and with a reasonable cost. So far, a number of approaches have been proposed to reconstruct one-dimensional or multi-dimensional spectrum from a smaller number of data sets than the previous schemes require. The first example of such *time-saving* protocols is the maximum entropy method (MEM), which was originally developed in astrophysics[30]. Its application to NMR spectroscopy was first reported by Sibisi and co-workers[31,32]. MEM soon found wide applications[33–37], and was combined with non-uniform sampling (NUS) scheme[38,39]. Since then, NUS

has attracted considerable interest, and has been incorporated into various protocols. Other noteworthy schemes include the Hadamard spectroscopy[40–44], reduced dimensionality[45–50], single scan two-dimensional spectroscopy or ultrafast two-dimensional spectroscopy[51–54], GFT NMR[55–57], covariance spectroscopy[58,59], recursive multidimensional decomposition (R-MDD)[60], compressed sensing[61–66], radial sampling[67], noise and artifact suppression using resampling (NASR)[68], and so on.

Even though these methods make full use of mathematics and may look formidable to NMR researchers majoring in chemistry, they are all valuable in the sense that they lifted up the limitation of NMR spectroscopy, enabling us to gain such chemical information that has not been accessible so far. In particular, the idea of covariance NMR, put forth by Brüschweiler and Zhang in solution NMR[58], has lead to a number of recent applications. The purpose of this review is to summarize recent works on covariance NMR, focusing on its applications to solid-state NMR spectroscopy. In Section 2, we overview the concept of covariance NMR, leaving at the end of the section an open question on what the author call "inner-product" NMR spectroscopy. Section 3 introduces applications of covariance NMR to solid-state systems of chemical/biological interest. In Section 4, we review sampling schemes that make the time-saving covariance NMR spectroscopy further time-saving. Section 5 is devoted to describe various variants of covariance NMR spectroscopy.

2 Overview of covariance NMR spectroscopy

In this section, we take a brief look at what the covariance NMR spectroscopy is. For more detailed and complete description, the reader may refer to the

pioneering paper published by Brüschweiler[59].

The main arena in which covariance NMR is used is two-dimensional (2D) correlation spectroscopy[69]. For a simple example, let us consider a three spin system consisting of spins A, B, and C, as schematically depicted in Fig. 1(a), and suppose that spins A and B are relatively close to each other, whereas spin C is at a distance, so that J/dipolar interactions are effective only between A and B. One can employ the conventional 2D Fourier Transform (2D-FT) NMR to obtain a 2D spectrum that looks like the one in Fig. 1(b), where the cross peak tells the existence of the correlation, and thereby the spatial proximity, between the relevant spins. Such information is very useful, as it provides structure constraint that can be used for, e.g., studies of higher order structure of biomolecules.

One possible and frequent problem with 2D-FT is that relatively a large number of data arrays need to be acquired, since the spectral resolution along the indirect dimension is determined by the number of the data arrays. In particular, when the signal-to-noise ratio of the individual free induction decays (FIDs) is low, as is often the case, signal averaging over many times is necessary for each evolution time, making the overall experimental time even longer. It is not unusual for one to spend several days or more, just to obtain a single 2D-FT spectrum. However, in order to improve the throughput of research, it is highly desirable to employ more efficient ways that can be used to extract the necessary information sooner.

In covariance NMR spectroscopy, pulse sequences to be used is the same as those in 2D-FT, but much fewer amounts of data sets along the indirect dimension suffice to produce a 2D spectrum similar to that obtained with 2D-FT.

Covariance is a concept in statistics, giving a measure of how much a pair of variables change in a correlated way. To explain the idea proposed by Brüschweiler of applying the covariance processing to NMR, let us suppose that we have an array of one-dimensional spectra obtained with incremented evolution time, as schematically described in Fig. 2. In this example, we have a homonuclear system of three spins, labeled with i, j, and k. For peak i and peak j, the ways that the peak amplitudes change with the evolution time look different. It follows that the covariance between i and j becomes very small. In contrast, peak i and peak k change in a similar way, resulting in a considerable covariance value. In this way, one can calculate a matrix, with its elements being the covariances between all possible pairs of the data points. The covariance spectrum looks quite similar to the traditional two-dimensional FT spectrum. One can tell the connectivity between the spins from the existence or absence of the cross peak, and from its intensity and mixing-time dependence.

To put the idea of covariance NMR spectroscopy using mathematical, thus unambiguous, expressions, let us consider a pair of vectors $X = (x_1, x_2, \cdots, x_n)$ and $Y = (y_1, y_2, \cdots, y_n)$. The covariance $C(X, Y)$ between X and Y is defined as

$$C(X,Y) = \frac{1}{n}\sum_{k=1}^{n}(x_k - \langle X\rangle)(y_k - \langle Y\rangle)^* \tag{1}$$

$$= \langle XY^*\rangle - \langle X\rangle\langle Y^*\rangle. \tag{2}$$

Here, the brakets and the asterisks denote mean values and complex conjugates. When we have a N_1 one-dimensional spectra $s_{k,m} = s(k\Delta t_1, m\Delta\omega_2)$ with $k = 1, 2, \cdots, N_1$ and $m = 1, 2, \cdots, N_2$, the covariance spectrum $\mathbf{C}$ is

obtained as a $N_2 \times N_2$ matrix, its (p, q) element $C_{p,q}$ being

$$C_{p,q} = \frac{1}{N_1} \sum_{k=1}^{N_1} (s_{k,p} - \langle s_p \rangle)(s_{k,q} - \langle s_q \rangle)^*, \tag{3}$$

where

$$\langle s_\xi \rangle = \frac{1}{N_1} \sum_{k=1}^{N_1} s_{k,\xi}. \tag{4}$$

On the other hand, the conventional 2D-FT spectrum $\mathbf{S}$ is calculated as

$$\mathbf{S}(p\Delta\omega_1, q\Delta\omega_2) = \sum_{p=0}^{N_1-1} s(p\Delta t_1, q\Delta\omega_2) \exp(-i\omega_1 p\Delta t_1). \tag{5}$$

The covariance spectrum $\mathbf{C}$ corresponds to the 2D-FT spectrum $\mathbf{S}$ *squared*, i.e., $S^T \cdot S$. Their similarity is based on the Parseval's theorem stating that, for functions $f(t)$ and $g(t)$ and their Fourier transformations $F(\omega)$ and $G(\omega)$, the following relationship holds:

$$\int_{-\infty}^{\infty} dt f(t) g^*(t) \propto \int_{-\infty}^{\infty} d\omega F(\omega) G^*(\omega). \tag{6}$$

In the present context, $s(t, p\Delta\omega_2)$ and $s(t, q\Delta\omega_2)$ correspond to $f(t)$ and $g(t)$, while $S(\omega, p\Delta\omega_2)$ and $S(\omega, q\Delta\omega_2)$ to $F(\omega)$ and $G(\omega)$, respectively. It follows that the square root $\mathrm{R} = \sqrt{\mathbf{C}}$ of the covariance matrix gives a 2D spectrum which can be used in the study of spin correlation, and thereby of higher-order structure, as is done in the conventional 2D-FT.

Importantly, in covariance, the spectral resolution in the indirect dimension is given by that in the direct dimension N_2. It follows that much smaller number of data length N_1 along the indirect dimension suffice to extract spin correlations than is required in the conventional 2D-FT scheme, so that one can significantly save the experimental time, or increase the number of signal accumulations within a given experimental time.

A straightforward way of calculating the square root $\mathbf{R}$ of the covariance

(square) matrix $\mathbf{C}$ is to apply diagonalization, i.e., to find such an orthogonal matrix $\mathbf{V}$ that

$$\mathbf{C} = \mathbf{V} \cdot \mathbf{D} \cdot \mathbf{V}^T, \tag{7}$$

where $\mathbf{D} = \mathrm{diag}(d_1, d_2, \cdots)$ is a diagonal matrix. The square root of the diagonal matrix is readily obtained as $\sqrt{\mathbf{D}} = \mathrm{diag}(\sqrt{d_1}, \sqrt{d_2}, \cdots)$, from which $\mathbf{R} = \sqrt{\mathbf{C}}$ is calculated to be

$$\mathbf{R} = \mathbf{V}^T \cdot \sqrt{\mathbf{D}} \cdot \mathbf{V}. \tag{8}$$

In practice, however, matrix diagonalization is computationally expensive, and the calculation of $\mathbf{R}$ can take an intolerable long time even with a modern computer. The algorithm based on singular value decomposition (SVD) is an efficient alternative[70].

It should be kept in mind that, in practice, covariance processing is performed over a limited, relatively short acquisition lengths N_1 in the indirect dimension, while the Parseval's theorem requires the integral to be performed over an *infinite* range. Thus, the above interesting and noteworthy correspondence is not rigorous one. In addition, the equivalence between the covariance and the left hand side of Eq. (6) is assured only when the average of $s(t_1, \omega_2)$ over t_1 vanishes, as one can see from the definition of the covariance in Eq. (1). This is true in many cases where the peaks in the one-dimensional spectrum $s(t_1, \omega_2)$ oscillate with the evolution time t_1. This is, however, not always the case, when the indirect acquisition length N_1 is relatively small, as is usually the case for covariance NMR, or for peaks relatively close to the carrier frequency.

In this context, one may be tempted to employ, instead of covariance, *another measure* of correlation between a pair of variables X and Y by discarding the

mean value in the definition of the covariance in Eq. (1),

$$I(X,Y) = \frac{1}{n}\sum_{k=1}^{n} x_k y_k^* \tag{9}$$

In linear algebra, $I(X,Y)$ is called as *an inner product*, or *a scalar product* of n-dimensional vectors X and Y^*. Using the inner product, the two-dimensional correlation spectrum can be constructed in the same way as in the case of covariance, and the Parseval's theorem can be straightforwardly applied without having to make the (sometimes invalid) assumption of vanishing mean values. Comparison between the covariance and the inner product has not been explored, and the question of whether the latter is superior or not for the NMR purposes is an open issue that require further studies. The idea of "inner-product NMR spectroscopy" is thus outside the scope of this review, and will not be discussed further here.

3 Applications of solid-state covariance NMR spectroscopy

In liquid solutions, nuclear spins are correlated through J-couplings, whereas in solids dipolar interactions come into play as well. The first report on the application of covariance to solid-state NMR was published by Hu et al., in which an "indirect" covariance homonuclear correlation spectrum was obtained from a 2D-FT heteronuclear correlation spectrum. The indirect covariance scheme, which will be discussed in section 5.1, contrasts with the original "direct" covariance spectroscopy, where the covariance processing is performed over an array of one-dimensional spectra.

3.1 Inorganic materials

Hu et al., also reported on the first application of *direct* covariance spectroscopy to solid-state NMR to reveal ^{13}C-^{13}C correlations in amino acids, ^{31}P-^{31}P correlations in alumino phosphates, and ^{29}Si-^{29}Si correlations in sodium borosilicate glass and silicalite-1. Interestingly, they demonstrated covariance processing in double-quantum correlation experiments employing POST-C7[71], BABA[72], and INADEQUATE[73]. In double-quantum 2D spectroscopy, time evolution along the indirect dimension is characterized by the frequencies given by the sum of the chemical shifts between the correlated spins, so that horizontal pairs of correlation peaks appear, as shown in Fig. 3. There, 125 data sets were acquired with a step of 12.5 us, Thus, the coherence profile during the evolution time was truncated at 1.6 ms.

During the evolution time, the quantum states of the relevant spin pair change in a *correlated* way, because they both involve oscillation at a *common* frequency corresponding to the sum of the chemical shifts. It follows that covariance processing can be used to measure the double-quantum correlation. Fig. 4(A) shows a 2D covariance spectrum using the same data source as in the conventional double-quantum spectrum (Fig. 3). Now, the double-quantum correlations appear as cross peaks. Importantly, the spectral resolution along the indirect dimension is given by that along the direct dimension, and fewer number of data sets suffice to obtain the desired correlations. It is impressive to see that the 2D covariance spectrum obtained with only 25 t_1 increments keeps the spectral feature, as demonstrated in Fig. 4(B).

With the covariance approach, experiments requiring an impractically long

measurement time can become realistic. An example of such is also demonstrated in Ref. [74], in which natural abundance ^{29}Si INADEQUATE experiment was carried out in silicate-1. Due to the low sensitivity and low natural abundance (ca. 4%) of ^{29}Si, the low efficiency of INADEQUATE transfer, and the relatively short transverse relaxation time in the direct dimension, only a limited number of data sets (32) could be acquired. Nevertheless, the covariance-processed 2D spectrum showed enough resolution to extract through-bond ^{29}Si-^{29}Si connectivity, as demonstrated in Fig. 5. There, cross peaks showing through-bond connectivity are clearly visible between sites 1, 2, and 3, while site 4 was found to be isolated from the others. Hu et al. claimed that such information was difficult to obtain with the conventional approach, which would take a very long time.

3.2 Biological solids

The earliest application of covariance spectroscopy to a complex biological system in the solid state was reported by Weingarth et al.[75]. In a ^{13}C,^{15}N-labeled microcrystalline sample of 85-residue domain-swapped homodimer of catabolite repression phosphocarrier protein, known as Crh, Weingarth et al. successfully observed covariance cross peaks showing long-range correlations that were buried in the noise in the 2D-FT spectrum. The correlation spectrum of such a relatively large molecule (molecular weight of Crh is 10.4 kDa per monomer) is crowded with cross peaks, so that insufficient spectral resolution, in particular along the indirect dimension, can be a serious problem in 2D-FT.

Fig. 6 compares covariance and 2D-FT spectra obtained from a common data set. The covariance spectra (a) and (c), which were obtained from 512 and

256 FIDs, showed no discernible difference, while the corresponding 2D-FT spectra (b) and (d) suffered from considerable degradation of spectral resolution. The covariance spectrum shown Fig. 7(a) reveals long-range, structurally important cross peaks. For example, the cross peak between the 61 (Val) and the 6 (Val) residues indicates their intermolecular proximity in the domain-swapped dimer. The cross peak between the 61 (Val) and the 37 (Lys) residues arises from intramolecular correlation. These cross peaks were invisible in the 2D-FT spectrum (Fig. 7(c)).

Another example in which covariance is applied to biological solid-state NMR was reported by Masuda et al., who studied interaction sites of curcumin and 42-residue amyloid β protein fibrils[76]. Curcumin is a food component in the rhizome of turmeric. It has attracted attention in the study of Alzheimer's disease (AD), since curcumin is known to prevent 42-residue amyloid-β protein (Aβ42) from aggregating into the fibrils that are responsible for the pathodology of AD. Moreover, the toxic Aβ42 fibrils disaggregate in the presence of curcumin. It is therefore important to investigate how curcumin interacts with the Aβ42 fibrils, and cause disaggregation of the latter.

The disorderd nature of the material leaves solid-state NMR as a unique analytical tool. Masuda et al. tackled the problem of characterizing the binding mode of the curcumin molecules to the Aβ42 fibrils using ^{13}C-^{13}C correlation scheme in combination with elaborate isotope labeling of the complex. As described in Fig. 8, Masuda et al. prepared a pair of separate, ^{13}C-labeled Aβ42 samples, each of which was mixed with curcumin labeled with ^{13}C at the aromatic sites. Analysis by the conventional 2D-FT approach was challenging due to the low sensitivity, and accordingly, they employed the covariance approach to successfully reveal magnetization transfer among the ^{13}C spins in

the curcumin molecules and the Aβ fibrils (Fig. 9).

It should be kept in mind that the covariance spectrum can contain "false" cross peaks, which have intensities larger than the noise level but have nothing to do with spin correlation. Such an artifact is caused by the nature of the covariance processing, and presumably, can be one of possible origins of reluctance of some researchers to employ the covariance approach. Nevertheless, one can readily identify the false cross peaks in many cases where correlation experiments are performed with various mixing times. The artifacts should not be affected by the mixing time, and from the viewpoint of evaluating the connectivity, mere existence of the cross peaks is of less importance compared to how they grow with the mixing time. In Ref. [76], Masuda et al. carefully confirmed that the cross peaks they observed in the covariance spectra were indeed the "real" cross peaks originating from the ^{13}C-^{13}C magnetization exchanges, by examining the mixing-time dependence of the cross-peak intensities (Fig. 10). In addition, they studied the mixing-time dependence based on a two-site exchange model and numerical simulations (supplementary material of Ref. [76]).

Aside from the powerfulness of the covariance approach, care should be taken when one tries to deduce scientific discussions from the data. Masuda et al. showed that curcumin interacts with the residues from 17 to 21, and the 12th residue in the N-terminal β-sheet. In a later report by Mithu et al.[77], the 12th residue was shown to be affected by curcumin, while they found no evidence for the binding between curcumin and residues 19-20, which were the only isotope-labeled residues in the region 17-21. The discrepancy was ascribed to different sample preparation schemes. This implies that the biniding mode can strongly depend on the way that curcumin is dosed.

Other applications of covariance NMR include natural abundance deuterium NMR spectroscopy in chiral polypeptide liquid crystals[78] and three-dimensional experiments of combined homonuclear spin-exchange and separated-local-field spectroscopies[79]. These works also presented new sampling schemes, and will be introduced in the next section.

4 Improvement of covariance toward further time-saving

4.1 NUS

The idea of non-uniform sampling (NUS) has found considerable interest and applications in the context of the conventional 2D-FT schemes. NUS is also compatible with the covariance spectroscopy. Lafon et al. reported on natural abundance deuterium NMR spectroscopy of 2-ethyloxirane (C_4H_8O) and methyl vernoleate ($C_{19}H_{34}O_3$) dissolved in chiral polypeptide liquid crystals (PBLG/$CHCl_3$ mixture), making comparison of Q-COSY Fz[80,81] datasets processed by the conventional 2D-FT, uniform sampling (US) covariance, and NUS covariance schemes[78]. Fig. 11(b) shows a ^{2}H Q-COSY Fz spectrum of 2-ethyloxirane (Fig 11(a)) obtained from 268 t_1-incremented FIDs with the conventional, US-FT scheme. As the length of the data array was decreased intentionally for a demonstrative purpose, the spectral resolution along the indirect dimension was reduced (Fig. 11(c)-(e)). When US-FT was replaced by the covariance processing, the spectral feature was kept, while noticeable reduction in the signal-to-noise was found (Fig. 11(f)-(h)). When Lafon et al. employed covariance with non-uniform sampling, the quality of the spectrum was virtually the same, even with the decrease in the data length by more

than five times.

It should be noted that the diagonal peaks are absent in the ^{2}H Q-COSY Fz spectrum (Fig. 11(b)). This means that even the relevant peak pairs evolve with different frequencies during t_1. The simple covariance processing would lead to a spectrum containing only diagonal peaks, so that no information can be extracted. This problem can be avoided by using what Lafon et al. call the *regularization* procedure, in which artificial diagonal-peak components are added in advance to the covariance processing, and afterwards, the diagonal peaks are subtracted. In this way, the covariance spectra in Fig. 11 were obtained.

4.2 Accumulation profile

In general, the nuclear magnetization decreases with the indirect evolution time t_1. In many (though not all) cases, the decaying profile is well approximated by an exponential function. Such a feature could be exploited to optimize the efficiency of data acquisition. Li et al. proposed to vary the number of signal accumulation with t_1 in accordance with a Gaussian function[82,83], making comparison between the Gaussian accumulation profile and the conventional square profile under the restriction that the signal decays exponentially with t_1. In addition, they examined the two options for the sampling interval, the uniform and non-uniform schemes (Fig. 12). As a result of their in-depth analysis, Li et al. came to the conclusion that the Gaussian accumulation profile with uniform sampling leads to the optimal result (Fig. 13).

4.3 Alternative States sampling

For structual determination of biopolymers, multi-dimensional (three or more) NMR spectroscopy is helpful, as the spectrum carries a number of distance and angle restraints. In the conventional scheme, requirement for the signal-to-noise ratio of the resonance line is demanding, limiting its application to samples whose resonance lines are relatively sharp and thereby the sensitivity is relatively good. Lin and Opella demonstrated the feasibility of three-dimensional experiments of combined homonuclear spin-exchange and separated-local-field spectroscopies even for the resonance lines with insufficient signal-to-noise ratio of less than 10[79]. Their successful 3D spectral reconstruction is ascribed to, in addition to the usage of covariance processing and compressed sensing, what Lin an Opella call the alternative States sampling scheme.

In the alternative States sampling scheme, real and imaginary part of the signals are sampled *alternately*, as described schematically in Fig. 14. Compared to the conventional States scheme[84,69], the experimental time is halved. At the same time, one can keep up with the profile of spin-magnetization evolution, when the covariance processing is combined with alternative State sampling. Fig. 15 demonstrates a ^{1}H-^{15}N/^{15}N/^{15}N three dimensional experiment performed in a single crystal sample of ^{15}N-labeled N-acetyl leucine. There, 50 complex points were acquired using alternative States sampling for covariance processing to extract ^{15}N/^{15}N correlation, while 44 real points were collected in the ^{1}H-^{15}N dipolar coupling dimension for data reconstruction by compressed sensing.

5 Variants of solid-state covariance NMR spectroscopy

5.1 Indirect covariance

Indirect covariance spectroscopy was proposed by Zhang and Brüschweiler[85] soon after publication of their pioneering work on covariance spectroscopy[58]. Its application to solid-state NMR was reported a few years later by Hu et al[86]. The procedure of the indirect covariance spectroscopy starts with a 2D *Fourier-transformed* heteronuclear correlation (HETCOR) spectrum. This is in contrast to the original direct covariance spectroscopy, in which covariance processing is applied to an array of one-dimensional spectra, so that Fourier transformation is performed only with respect to the direct dimension. From a single I-S 2D HETCOR spectrum, a pair of homonuclear correlation (HOMCOR) spectra are obtained, each of which reflect the I-I (S-S) homonuclear connectivity *mediated by* the I-S heteronuclear correlation. It should be noted that a HOMCOR spectrum obtained by indirect covariance carries different information from that the conventional HOMCOR provides; only those homonuclear spin pairs correlated to a *common* heteronuclear spin will show cross peaks, and mere direct I-I (S-S) correlation without I-S correlation would be invisible.

To demonstrate solid-state indirect covariance spectroscopy, Hu et al. performed ^{27}Al-^{31}P SPAM-MQ-J-HETCOR in $AlPO_4$-14. During the indirect evolution time (t_1), the second-order ^{27}Al quadrupolar interactions were eliminated by MQMAS[87,88]. In addition, soft pulse added mixing (SPAM)[89] was employed to exploit multiple coherent transfer pathways, and thereby to improve the sensitivity. Then, the ^{27}Al magnetizations were transferred

to the ^{31}P nuclei through the ^{27}Al-^{31}P J couplings by a refocused INEPT technique[90–92]. The conventional 2D-FT resulted in a HETCOR spectrum shown in Fig. 16, from which indirect covariance ^{27}Al and ^{31}P spectra shown in Fig. 17 and Fig. 18 were obtained. Note that the pair of indirect covariance spectra do not give any extra information compared to the original HETCOR spectrum. Nevertheless, the former should provide an instructive viewpoint of the data, helping one to interpret the indirect connectivity.

5.2 Dual transformation

The noises in the FT spectrum and in the covariance spectrum are uncorrelated. Exploiting this fact, Kaiser et al. proposed a scheme to reduce noise[93]. In what they called the Dual Transformation Denoising (DTD) scheme, two copies of an identical data source are processed separately; one is Fourier-transformed, while the other is covariance-processed. Then, these two are multiplied into a single spectrum. A diagram of the DTD scheme is shown in Fig. 19. Kaiser et al. showed that the overall effect is to reduce the noise, or equivalently, decrease the measurement time required to attain a given signal-to-noise ratio. The superior sensitivity of the DTD spectrum to that of the FT spectrum is demonstrated in Fig. 20.

For structural analysis, one often needs to perform correlation experiments for various mixing times, since the mixing-time dependence of the cross-peak intensities provides important distance restrictions. Unfortunately, the cross peaks of the DTD spectrum build up with the mixing time in a somewhat different way from those in the FT spectrum. To retain the quantitative feature of the buildup curves, Kaiser et al. proposed a *template* DTD scheme[93].

In template DTD, covariance processing is performed only on the data acquired with the longest mixing time. Then, the individual FT spectra obtained whit various mixing times are multiplied by this common covariance spectrum (Fig. 21). As demonstrated in Fig. 22, the buildup curves of the template DTD spectra show similar behavior to those of the FT spectra.

5.3 HETCOR

Until recently, the scope of covariance NMR spectroscopy had been limited to homonuclear correlations (Note that, in indirect covariance spectroscopy, heteronuclear correlations are *used* to obtain homonuclear correlations.) Extension of covariance spectroscopy to include heteronuclear correlations was reported by Takeda et al., who showed that the covariance processing can be used to obtain heteronuclear correlations together with homonuclear correlations in ^{1}H-^{1}H dipolar-coupling mediated ^{13}C/^{15}N chemical shift correlation experiments using a ^{13}C/^{15}N dual-receiver system[94].

During implementation of a pulse sequence shown in Fig. 23, the ^{13}C and ^{15}N magnetizations evolved during t_1 are transferred to the ^{1}H spins, which undergo exchange via ^{1}H-^{1}H spin diffusion during the mixing time, and then sent back to the ^{13}C and ^{15}N spins. The simultaneously acquired ^{13}C/^{15}N FIDs using the dual-receiver system are first Fourier-transformed separately with respect to the direct dimension (t_2). Then, the one-dimensional ^{13}C and ^{15}N spectra and the *joined* together to form a *single* array of one-dimensional spectra, which is covariance-processed in the conventional manner. The resultant 2D spectrum consists of four regions corresponding to the ^{13}C-^{13}C, ^{13}C-^{15}N, ^{15}N-^{13}C, and ^{15}N-^{15}N correlations, as schematically depicted in Fig. 24 and

demonstrated in Fig. 25.

Even though the same data set can be used to obtain a pair of the conventional 2D-FT spectra (Fig. 23(a) and Fig. 25(c)(d)), the covariance-processed homonuclear/heteronuclear correlation spectrum retain the merits that have already been confirmed for the original covariance NMR spectroscopy; the spectral resolution along the indirect dimension is determined by that along the direct dimension. It follows that much fewer amounts of data sets suffice to yield a satisfactory spectrum, leading to a shorter experimental time, or a larger number of signal accumulations can be performed within a given experimental time.

5.4 phase covariance

So far, we have explored solid-state covariance NMR spectroscopy that allows for extracting spin correlations more efficiently than in the conventional 2D-FT approach. Since covariance gives a measure of how much a pair of variables are correlated with each other, it should be useful in other scenes of NMR spectroscopy as well. In this context, Fukazawa and Takegoshi proposed a method for statistical data processing based on the idea of what they call *phase covariance*[95], which challenges the very ordinary statistical procedure in NMR: signal accumulation or signal averaging. Instead of performing signal averaging over many times as usual, one records and stores the individual FID *separately*, which may be accompanied with phase increment of the rf pulse. Later on, the array of the data acquired in this way are used for post processing. The idea of phase covariance is schematically described in Fig. 26.

Even though phase covariance shares the term with covariance NMR spectroscopy, they are distinct from each other; the former deals with correlation between the phase of the rf pulse and that of the resonance line of a one-dimensional spectrum, while the latter concerns exchange of magnetizations between nuclear spins. For simplicity, we consider a single-pulse sequence with the phase of the rf pulse ϕ(Fig. 26(a)). Here, an array of *separate* one-dimensional spectra is obtained with consecutively incremented ϕ (Fig. 26(b)). We suppose that the NMR signal is present and absent at spectral positions A and B in Fig. 26(b). Then, point A ought to vary with the phase increment ϕ of the rf pulse, so that correlation between the spectral phase and rf-pulse phase results in diagonal distribution, as shown in Fig. 26(c).

In reality, the presence of the noise causes off-diagonal distribution (Fig. 27(b)), depending on the signal-to-noise ratio per scan. Point B, on the other hand, has no signal component and is thus uncorrelated with the rf phase, so that the distribution should be random (Fig. 26(d), Fig. 27(c)). The idea of phase covariance is to calculate covariance between the array of individual spectral position and the array of the phase values used in the experiment. An example of the spectrum obtained in this way is shown in Fig. 27(e), which appears quite similar to the one obtained from the conventional signal averaging (Fig. 27(d)). Since the profiles of the noise in these two spectra are not correlated, they can be multiplied into another spectrum with reduced noise, as shown in Fig. 27(f). Multiplication of spectra obtained from the same data source but with different processing is reminiscent of the idea proposed in the DTD scheme (see 5.2)[93]. Phase covariance was also shown to be efficient for eliminating incoherent spurious noises due to, e.g., radiation from other devices or broadcasting radio waves[96].

However, one technical difficulty arises from the periodicity of the phase. That is, in the distribution plot of the spectral-phase and pulse-phase, e.g., Fig. 27(b), considerable population is found in the upper-left and lower-right regions. The points in those regions cause decrease in the covariance value, even though they carry correlation between the spectral phase and the rf phase. To avoid this problem, Fukazawa et al. introduced an interesting transformation of the distribution map[96]. Here, instead of showing its full mathematical treatment, we take a look at the geometrical representation of the proposed transformation (Fig. 28). Let us consider a plane spanned by the spectral phase ($-\pi < \phi < \pi$) and the pulse phase ($-\pi < \psi < \pi$). The area is folded twice, horizontally (Fig. 28(a)), and then vertically (Fig. 28(b)). These operations correspond to taking absolute values with respect to ϕ and ψ, respectively. As a result, we have a folded area with the ranges $0 < \phi < \pi$ and $0 < \psi < \pi$ (Fig. 28(c)). Then, the origin is shifted by $(-\pi/2, -\pi/2)$ to complete the transformation (Fig. 28(d)). Its effect is to move the upper-left and the lower-right regions to the diagonal region, while the diagonal line is kept diagonal. It follows that one can fully exploit $\phi - \psi$ correlation carried by the individual points in the phase-covariance processing.

6 Summary

In this article, we have reviewed the covariance approach — one promising strategy toward efficient acquisition of information from a limited number of data sets. We have seen the fruitful outcomes of covariance NMR spectroscopy, including its applications to solid-state NMR studies of chemically or biologically important systems, its improvements to enhance the efficiency

further, and its modifications to accomodate various needs of structural analysis. In addition, the question regarding to the inner-product spectroscopy, to be answered in future studies, has been posted. At the moment of writing this review, covariance NMR spectroscopy is rather young and the number of relevant papers is not many. From the author's perspective, the covariance scheme will gain substantial popularity, simply because it is very useful. Just like Fourier-transformation NMR, which had been established a few decades after the dawn of NMR, has now been a very ordinary, routine procedure, covariance NMR could be another common and standard methodology in the future. Even though the mathematics of covariance may look formidable, it is *not* more difficult than the mathematics of Fourier analysis is; it would simply be a matter of getting used to it. As a final remark, it is interesting to note that the papers cited in this review article drew attention in the context of general two-dimensional correlation spectroscopy[97] as well as of NMR, which is *a branch* of spectroscopy.

Acknowledgment

I am grateful to Yuichi Masuda, Tatsuya Yatagawa, Yasushi Kusakabe, Yasuto Noda, Masashi Fukuchi, K. Takegoshi, Olivier Lafon, Julien Trébosc, and Jean-Paul Amoureux for giving me opportunities to enjoy exploring solid-state covariance NMR spectroscopy. I thank Yasushi Kusakabe for his comments and suggestions.

References

[1] A. Abragam, M. Goldman, Principles of dynamic nuclear polarisation, Reports on Progress in Physics 41 (3) (1978) 395–467. doi:10.1088/0034-4885/41/3/002.

[2] R. Tycko, J. A. Reimer, Optical Pumping in Solid State Nuclear Magnetic Resonance, The Journal of Physical Chemistry 100 (31) (1996) 13240–13250. doi:10.1021/jp953667u.

[3] J. Haupt, A new effect of dynamic polarization in a solid obtained by rapid change of temperature, Physics Letters A 38 (6) (1972) 389–390. doi:10.1016/0375-9601(72)90219-8.

[4] S. Clough, Thermally induced nuclear dipolar polarization, Physics Letters A 42 (5) (1973) 371–372. doi:10.1016/0375-9601(73)90377-0.

[5] A. J. Horsewill, Quantum tunnelling aspects of methyl group rotation studied by NMR, Progress in Nuclear Magnetic Resonance Spectroscopy 35 (4) (1999) 359–389. doi:10.1016/S0079-6565(99)00016-3.

[6] M. Tomaselli, C. Degen, B. H. Meier, Haupt magnetic double resonance, The Journal of Chemical Physics 118 (19) (2003) 8559. doi:10.1063/1.1573635.

[7] M. Tomaselli, U. Meier, B. H. Meier, C. Zu, Tunneling-induced spin alignment at low and zero field., Journal of Chemical Physics 120 (9) (2004) 4051–4054. doi:10.1063/1.1649315.

[8] M. Icker, S. Berger, Unexpected multiplet patterns induced by the Haupt-effect., Journal of Magnetic Resonance 219 (2012) 1–3. doi:10.1016/j.jmr.2012.03.021.

[9] P. Styles, N. Soffe, C. Scott, D. Crag, F. Row, D. White, P. White, A high-resolution NMR probe in which the coil and preamplifier are cooled with liquid helium, Journal of Magnetic Resonance 60 (3) (1984) 397–404. doi:10.1016/0022-2364(84)90050-7.

[10] P. Styles, N. F. Soffe, C. A. Scott, An improved cryogenically cooled probe for high-resolution NMR, Journal of Magnetic Resonance 84 (2) (1989) 376–378. doi:10.1016/0022-2364(89)90383-1.

[11] H. Kovacs, D. Moskau, M. Spraul, Cryogenically cooled probes—a leap in NMR technology, Progress in Nuclear Magnetic Resonance Spectroscopy 46 (2-3) (2005) 131–155. doi:10.1016/j.pnmrs.2005.03.001.

[12] A. S. Hall, B. Barnard, P. McArthur, D. J. Gilderdale, I. R. Young, G. M. Bydder, Investigation of a whole-body receiver coil operating at liquid nitrogen temperatures, Magnetic Resonance in Medicine 7 (2) (1988) 230–235. doi:10.1002/mrm.1910070211.

[13] L. Darrasse, Perspectives with cryogenic RF probes in biomedical MRI, Biochimie 85 (9) (2003) 915–937. doi:10.1016/j.biochi.2003.09.016.

[14] T. Mizuno, K. Hioka, K. Fujioka, K. Takegoshi, Development of a magic-angle spinning nuclear magnetic resonance probe with a cryogenic detection system for sensitivity enhancement., Review of Scientific Instruments 79 (4) (2008) 044706. doi:10.1063/1.2912946.

[15] T. Mizuno, K. Takegoshi, Development of a cryogenic duplexer for solid-state nuclear magnetic resonance., Review of Scientific Instruments 80 (12) (2009) 124702. doi:10.1063/1.3263908.

[16] K. R. Thurber, R. Tycko, Biomolecular solid state NMR with magic-angle spinning at 25K., Journal of Magnetic Resonance 195 (2) (2008) 179–186. doi:10.1016/j.jmr.2008.09.015.

[17] Ē. Kupče, R. Freeman, B. K. John, Parallel Acquisition of Two-Dimensional NMR Spectra of Several Nuclear Species, Journal of the American Chemical Society 128 (2006) 9606–9607.

[18] Ē. Kupče, R. Freeman, Parallel receivers and sparse sampling in multidimensional NMR, Journal of Magnetic Resonance 213 (2011) 1–13. doi:10.1016/j.jmr.2011.08.027.

[19] D. L. Olson, T. L. Peck, A. G. Webb, R. L. Magin, J. V. Sweedler, High-Resolution Microcoil 1H-NMR for Mass-Limited, Nanoliter-Volume Samples, Science 270 (1995) 1967–1970.

[20] T. L. Peck, R. L. Magin, P. C. Lauterbur, Design and Analysis of Microcoils for NMR Microscopy, Journal of Magnetic Resonance B108 (1995) 114–124.

[21] H. Janssen, A. Brinkmann, E. R. H. van Eck, P. J. M. van Bentum, A. P. M. Kentgens, Microcoil high-resolution magic angle spinning NMR spectroscopy., Journal of the American Chemical Society 128 (27) (2006) 8722–8723. doi:10.1021/ja061350+.

[22] D. Sakellariou, G. Le Goff, J.-F. Jacquinot, High-resolution, high-sensitivity NMR of nanolitre anisotropic samples by coil spinning., Nature 447 (7145) (2007) 694–697. doi:10.1038/nature05897.

[23] A. P. M. Kentgens, J. Bart, P. J. M. van Bentum, A. Brinkmann, E. R. H. van Eck, J. G. E. Gardeniers, J. W. G. Janssen, P. Knijn, S. Vasa, M. H. W. Verkuijlen, High-resolution liquid- and solid-state nuclear magnetic resonance of nanoliter sample volumes using microcoil detectors., Journal of Chemical Physics 128 (5) (2008) 052202. doi:10.1063/1.2833560.

[24] K. Takeda, Microcoils and microsamples in solid-state NMR, Solid State Nuclear Magnetic Resonancee 47-48 (2012) 1–9.

[25] D. Rugar, C. Yannoni, J. Sidles, Mechanical detection of magnetic resonance, Nature 360 (1992) 563–566.

[26] D. Rugar, O. Züger, S. Hoen, C. Yannoni, H.-M. Vieth, R. Kendrick, Force Detection of Nuclear Magnetic Resonance, Science 264 (1994) 1560–1563.

[27] L. A. Madsen, G. M. Leskowitz, D. P. Weitekamp, Observation of force-detected nuclear magnetic resonance in a homogeneous field., PNAS 101 (35) (2004) 12804–12808. doi:10.1073/pnas.0405232101.

[28] S. Kuehn, S. a. Hickman, J. a. Marohn, Advances in mechanical detection of magnetic resonance., Journal of Chemical Physics 128 (5) (2008) 052208. doi:10.1063/1.2834737.

[29] C. L. Degen, M. Poggio, H. J. Mamin, C. T. Rettner, D. Rugar, Nanoscale magnetic resonance imaging., PNAS 106 (5) (2009) 1313–1317. doi:10.1073/pnas.0812068106.

[30] S. Gull, G. Daniell, Image reconstruction from incomplete and noisy data, Nature 272 (5655) (1978) 686–690. doi:10.1038/272686a0.

[31] S. Sibisi, Two-dimensional reconstructions from one-dimensional data by maximum entropy, Nature 301 (5896) (1983) 134–136. doi:10.1038/301134a0.

[32] S. Sibisi, J. Skilling, R. G. Brereton, E. D. Laue, J. Staunton, Maximum entropy signal processing in practical NMR spectroscopy, Nature 311 (5985) (1984) 446–447. doi:10.1038/311446a0.

[33] E. Laue, M. Mayger, J. Skilling, J. Staunton, Reconstruction of phase-sensitive two-dimensional NMR spectra by maximum entropy, Journal of Magnetic Resonance 68 (1) (1986) 14–29. doi:10.1016/0022-2364(86)90312-4.

[34] E. Laue, J. Skilling, J. Staunton, Maximum entropy reconstruction of spectra containing antiphase peaks, Journal of Magnetic Resonance 63 (2) (1985) 418–424. doi:10.1016/0022-2364(85)90338-5.

[35] P. Hore, NMR data processing using the maximum entropy method, Journal of Magnetic Resonance 62 (3) (1985) 561–567. doi:10.1016/0022-2364(85)90229-X.

[36] J. C. Hoch, Maximum entropy signal processing of two-dimensional NMR

data, Journal of Magnetic Resonance 64 (3) (1985) 436–440. doi:10.1016/0022-2364(85)90106-4.

[37] E. D. Lade, J. Skilling, J. Staunton, S. Sibisi, R. G. Brereton, Maximum entropy method in nuclear magnetic resonance spectroscopy, Journal of Magnetic Resonance 62 (3) (1985) 437–452. doi:10.1016/0022-2364(85)90213-6.

[38] J. Barna, E. Laue, M. Mayger, J. Skilling, S. Worrall, Exponential sampling, an alternative method for sampling in two-dimensional NMR experiments, Journal of Magnetic Resonance 73 (1) (1987) 69–77. doi:10.1016/0022-2364(87)90225-3.

[39] A. S. Stern, K.-B. Li, J. C. Hoch, Modern Spectrum Analysis in Multidimensional NMR Spectroscopy: Comparison of Linear-Prediction Extrapolation and Maximum-Entropy Reconstruction, Journal of the American Chemical Society 124 (9) (2002) 1982–1993. doi:10.1021/ja011669o.

[40] J. Ashida, T. Nakai, T. Terao, 1D NMR Separation of overlapping powder patterns by selective rf irradiation and switching-angle spinning, Chemical Physics Letters 168 (6) (1990) 523–528. doi:10.1016/0009-2614(90)85664-X.

[41] V. Blechta, R. Freeman, Multi-site Hadamard NMR spectroscopy, Chemical Physics Letters 215 (4) (1993) 341–346. doi:10.1016/0009-2614(93)85725-4.

[42] Ē. Kupče, R. Freeman, Fast multi-dimensional Hadamard spectroscopy, Journal of Magnetic Resonance 162 (1) (2003) 56–63. doi:10.1016/S1090-7807(03)00036-3.

[43] Ē. Kupče, T. Nishida, R. Freeman, Hadamard NMR spectroscopy, Progress in Nuclear Magnetic Resonance Spectroscopy 42 (3-4) (2003) 95–122. doi:10.1016/S0079-6565(03)00022-0.

[44] J. Ashida, Ē. Kupče, J.-P. Amoureux, Hadamard NMR spectroscopy in solids., Journal of Magnetic Resonance 178 (1) (2006) 129–35. doi:10.1016/j.jmr.2005.09.001.

[45] T. Szyperski, G. Wider, J. H. Bushweller, K. Wuethrich, Reduced dimensionality in triple-resonance NMR experiments, Journal of the American Chemical Society 115 (20) (1993) 9307–9308. doi:10.1021/ja00073a064.

[46] B. Brutscher, J. Simorre, M. Caffrey, D. Marion, Design of a Complete Set of Two-Dimensional Triple-Resonance Experiments for Assigning Labeled Proteins, Journal of Magnetic Resonance B105 (1) (1994) 77–82. doi:10.1006/jmrb.1994.1104.

[47] T. Szyperski, D. Braun, C. Fernandez, C. Bartels, K. Wuthrich, A Novel Reduced-Dimensionality Triple-Resonance Experiment for Efficient Polypeptide Backbone Assignment, 3D HN N, Journal of Magnetic Resonance B108 (2) (1995) 197–203. doi:10.1006/jmrb.1995.1124.

[48] K. Ding, A. M. Gronenborn, Novel 2D Triple-Resonance NMR Experiments for Sequential Resonance Assignments of Proteins, Journal of Magnetic Resonance 156 (2) (2002) 262–268. doi:10.1006/jmre.2002.2537.

[49] Ē. Kupče, R. Freeman, Projection-reconstruction technique for speeding up multidimensional NMR spectroscopy., Journal of the American Chemical Society 126 (20) (2004) 6429–6240. doi:10.1021/ja049432q.

[50] J. G. Reddy, R. V. Hosur, Reduced Dimensionality (4,3)D-HN(C)NH for Rapid Assignment of 1HN-15N HSQC Peaks in Proteins: An Analytical Tool for Protein Folding, Proteomics, and Drug Discovery Programs, Analytical Chemistry 84 (2012) 10404–10410.

[51] L. Frydman, T. Scherf, A. Lupulescu, The acquisition of multidimensional NMR spectra, PNAS 99 (25) (2002) 15858–15862.

[52] L. Frydman, A. Lupulescu, T. Scherf, Principles and features of single-scan two-dimensional NMR spectroscopy., Journal of the American Chemical Society 125 (30) (2003) 9204–9217. doi:10.1021/ja030055b.

[53] M. Gal, M. Mishkovsky, L. Frydman, Real-time monitoring of chemical transformations by ultrafast 2D NMR spectroscopy., Journal of the American Chemical Society 128 (3) (2006) 951–956. doi:10.1021/ja0564158.

[54] L. Frydman, D. Blazina, Ultrafast two-dimensional nuclear magnetic resonance spectroscopy of hyperpolarized solutions, Nature Physics 3 (6) (2007) 415–419. doi:10.1038/nphys597.

[55] S. Kim, T. Szyperski, GFT NMR, a new approach to rapidly obtain precise high-dimensional NMR spectral information., Journal of the American Chemical Society 125 (5) (2003) 1385–1393. doi:10.1021/ja028197d.

[56] S. Kim, T. Szyperski, GFT NMR experiments for polypeptide backbone and 13 Cβ chemical shift, Journal of Biomolecular NMR 28 (2004) 117–130.

[57] H. S. Atreya, T. Szyperski, G-matrix Fourier transform NMR spectroscopy for complete protein resonance assignment., PNAS 101 (26) (2004) 9642–9647. doi:10.1073/pnas.0403529101.

[58] R. Brüschweiler, F. Zhang, Covariance nuclear magnetic resonance spectroscopy., Journal of Chemical Physics 120 (11) (2004) 5253–5260. doi:10.1063/1.1647054.

[59] R. Brüschweiler, Theory of covariance nuclear magnetic resonance spectroscopy., Journal of Chemical Physics 121 (1) (2004) 409–414. doi:10.1063/1.1755652.

[60] V. Jaravine, I. Ibraghimov, V. Y. Orekhov, Removal of a time barrier for high-resolution multidimensional NMR spectroscopy, Nature Methods 3 (8) (2006) 605–607. doi:10.1038/NMETH900.

[61] E. J. Candès, J. Romberg, T. Tao, Robust Uncertainty Principles : Exact Signal Frequency Information, IEEE Transaction on Information Theory 52 (2) (2006) 489–509.

[62] M. Lustig, D. Donoho, J. M. Pauly, Sparse MRI: The application of compressed sensing for rapid MR imaging., Magnetic Resonance in Medicine 58 (6) (2007) 1182–1195. doi:10.1002/mrm.21391.

[63] S. Hu, M. Lustig, A. P. Chen, J. Crane, A. Kerr, D. a. C. Kelley, R. Hurd, J. Kurhanewicz, S. J. Nelson, J. M. Pauly, D. B. Vigneron, Compressed sensing for resolution enhancement of hyperpolarized 13C flyback 3D-MRSI., Journal of magnetic resonance (San Diego, Calif. : 1997) 192 (2) (2008) 258–64. doi:10.1016/j.jmr.2008.03.003.

[64] K. Kazimierczuk, A. Zawadzka, W. Koźmiski, Narrow peaks and high dimensionalities: exploiting the advantages of random sampling., Journal of Magnetic Resonance 197 (2) (2009) 219–228. doi:10.1016/j.jmr.2009.01.003.

[65] M. W. Maciejewski, H. Z. Qui, I. Rujan, M. Mobli, J. C. Hoch, Nonuniform sampling and spectral aliasing., Journal of Magnetic Resonance 199 (1) (2009) 88–93. doi:10.1016/j.jmr.2009.04.006.

[66] K. Kazimierczuk, V. Y. Orekhov, Accelerated NMR spectroscopy by using compressed sensing., Angewandte Chemie 50 (24) (2011) 5556–5559. doi:10.1002/anie.201100370.

[67] B. E. Coggins, R. A. Venters, P. Zhou, Radial sampling for fast NMR: Concepts and practices over three decades., Progress in Nuclear Magnetic Resonance Spectroscopy 57 (4) (2010) 381–419. doi:10.1016/j.pnmrs.2010.07.001.

[68] B. Jiang, F. Luo, Y. Ding, P. Sun, X. Zhang, L. Jiang, C. Li, X.-a. Mao, D. Yang, C. Tang, M. Liu, NASR: an effective approach for simultaneous noise and artifact suppression in NMR spectroscopy., Analytical chemistry 85 (4) (2013) 2523–2528. doi:10.1021/ac303726p.

[69] R. R. Ernst, G. Bodenhausen, A. Wokaun, Principles of Nuclear Magnetic Resonance in One and Two Dimensions, Oxford University Press, 1987.

[70] N. Trbovic, S. Smirnov, F. Zhang, R. Brüschweiler, Covariance NMR spectroscopy by singular value decomposition., Journal of Magnetic Resonance 171 (2) (2004) 277–283. doi:10.1016/j.jmr.2004.08.007.

[71] M. Hohwy, H. J. Jakobsen, M. Eden, M. H. Levitt, N. C. Nielsen, Broadband dipolar recoupling in the nuclear magnetic resonance of rotating solids: A compensated C7 pulse sequence, The Journal of Chemical Physics 108 (7) (1998) 2686–2694. doi:10.1063/1.475661.

[72] W. Sommer, J. Gottwald, D. Demco, H. Spiess, Dipolar Heteronuclear Multiple-Quantum NMR Spectroscopy in Rotating Solids, Journal of Magnetic Resonance, Series A 113 (1) (1995) 131–134. doi:10.1006/jmra.1995.1068.

[73] A. Bax, R. Freeman, S. P. Kempsell, Natural abundance carbon-13-carbon-13 coupling observed via double-quantum coherence, Journal of the American Chemical Society 102 (14) (1980) 4849–4851. doi:10.1021/ja00534a056.

[74] B. Hu, J.-P. Amoureux, J. Trebosc, M. Deschamps, G. Tricot, Solid-state NMR covariance of homonuclear correlation spectra., The Journal of Chemical Physics 128 (13) (2008) 134502. doi:10.1063/1.2884341.

[75] M. Weingarth, P. Tekely, R. Brüschweiler, G. Bodenhausen, Improving the quality of 2D solid-state NMR spectra of microcrystalline proteins by covariance analysis., Chemical Communications 46 (6) (2010) 952–954. doi:10.1039/b920844e.

[76] Y. Masuda, M. Fukuchi, T. Yatagawa, M. Tada, K. Takeda, K. Irie, K.-I. Akagi, Y. Monobe, T. Imazawa, K. Takegoshi, Solid-state NMR analysis of interaction sites of curcumin and 42-residue amyloid β-protein fibrils., Bioorganic & medicinal chemistry 19 (20) (2011) 5967–74. doi:10.1016/j.bmc.2011.08.052.

[77] V. S. Mithu, B. Sarkar, D. Bhowmik, A. K. Das, M. Chandrakesan, S. Maiti, P. K. Madhu, Curcumin Alters the Salt Bridge-containing Turn Region in

Amyloid β(1-42) Aggregates., The Journal of Biological Chemistry 289 (16) (2014) 11122–11131. doi:10.1074/jbc.M113.519447.

[78] O. Lafon, B. Hu, J.-P. Amoureux, P. Lesot, Fast and high-resolution stereochemical analysis by nonuniform sampling and covariance processing of anisotropic natural abundance 2D 2H NMR datasets., Chemistry - A European Journal 17 (24) (2011) 6716–6724. doi:10.1002/chem.201100461.

[79] E. C. Lin, S. J. Opella, Covariance spectroscopy in high-resolution multi-dimensional solid-state NMR., Journal of Magnetic Resonance 239 (2014) 57–60. doi:10.1016/j.jmr.2013.11.018.

[80] D. Merlet, B. Ancian, J. Courtieu, P. Lesot, Two-Dimensional Deuterium NMR Spectroscopy of Chiral Molecules Oriented in a Polypeptide Liquid Crystal: Applications for the Enantiomeric Analysis through Natural Abundance Deuterium NMR, Journal of the American Chemical Society 121 (22) (1999) 5249–5258. doi:10.1021/ja9837699.

[81] O. Lafon, P. Lesot, D. Merlet, J. Courtieu, Modified z-gradient filtering as a mean to obtain phased deuterium autocorrelation 2D NMR spectra in oriented solvents., Journal of Magnetic Resonance 171 (1) (2004) 135–142. doi:10.1016/j.jmr.2004.08.010.

[82] Y. Li, Q. Wang, Z. Zhang, J. Yang, B. Hu, Q. Chen, I. Noda, F. Deng, Covariance spectroscopy with a non-uniform and consecutive acquisition scheme for signal enhancement of the NMR experiments., Journal of Magnetic Resonance 217 (2012) 106–111. doi:10.1016/j.jmr.2012.02.016.

[83] Y. Li, B. Hu, Q. Chen, Q. Wang, Z. Zhang, J. Yang, I. Noda, J. Trébosc, O. Lafon, J.-P. Amoureux, F. Deng, Comparison of various sampling schemes and accumulation profiles in covariance spectroscopy with exponentially decaying 2D signals., The Analyst 138 (8) (2013) 2411–2419. doi:10.1039/c3an36375a.

[84] D. J. States, R. A. Haberkorn, D. J. Ruben, A two-dimensional nuclear overhauser experiment with pure absorption phase in four quadrants*1, Journal of Magnetic Resonance 48 (2) (1982) 286–292. doi:10.1016/0022-2364(82)90279-7.

[85] F. Zhang, R. Brüschweiler, Indirect covariance NMR spectroscopy., Journal of the American Chemical Society 126 (41) (2004) 13180–1. doi:10.1021/ja047241h.

[86] B. Hu, J.-P. Amoureux, J. Trebosc, Indirect covariance NMR spectroscopy of through-bond homo-nuclear correlations for quadrupolar nuclei in solids under high-resolution., Solid State Nuclear Magnetic Resonancee 31 (4) (2007) 163–168. doi:10.1016/j.ssnmr.2007.03.002.

[87] L. Frydman, J. S. Harwood, Isotropic Spectra of Half-Integer Quadrupolar Spins from Bidimensional Magic-Angle Spinning NMR, Journal of the American Chemical Society 117 (1995) 5367–5368.

[88] A. Medek, J. S. Harwood, L. Frydman, Multiple-Quantum Magic-Angle Spinning NMR: A New Method for the Study of Quadrupolar Nuclei in Solids, Journal of the American Chemical Society 117 (51) (1995) 12779–12787. doi:10.1021/ja00156a015.

[89] Z. Gan, H.-T. Kwak, Enhancing MQMAS sensitivity using signals from multiple coherence transfer pathways., Journal of Magnetic Resonance 168 (2) (2004) 346–351. doi:10.1016/j.jmr.2004.03.021.

[90] G. A. Morris, R. Freeman, Enhancement of nuclear magnetic resonance signals by polarization transfer, Journal of the American Chemical Society 101 (3) (1979) 760–762. doi:10.1021/ja00497a058.

[91] G. A. Morris, Sensitivity enhancement in nitrogen-15 NMR: polarization transfer using the INEPT pulse sequence, Journal of the American Chemical

Society 102 (1) (1980) 428–429. doi:10.1021/ja00521a097.

[92] D. Burum, R. Ernst, Net polarization transfer via a J-ordered state for signal enhancement of low-sensitivity nuclei, Journal of Magnetic Resonance (1969) 39 (1) (1980) 163–168. doi:10.1016/0022-2364(80)90168-7.

[93] C. Kaiser, J. J. Lopez, W. Bermel, C. Glaubitz, Dual transformation of homonuclear solid-state NMR spectra–an option to decrease measuring time., Biochimica et Biophysica Acta 1768 (12) (2007) 3107–3115. doi:10.1016/j.bbamem.2007.09.004.

[94] K. Takeda, Y. Kusakabe, Y. Noda, M. Fukuchi, K. Takegoshi, Homo- and heteronuclear two-dimensional covariance solid-state NMR spectroscopy with a dual-receiver system., Physical Chemistry Chemical Physics 14 (27) (2012) 9715–9721. doi:10.1039/c2cp41191a.

[95] J. Fukazawa, K. Takegoshi, Phase covariance in NMR signal., Physical Chemistry Chemical Physics 12 (37) (2010) 11225–11227. doi:10.1039/c0cp00644k.

[96] J. Fukazawa, K. Takeda, K. Takegoshi, Post-processing of individual signals for de-noising., Journal of Magnetic Resonance 211 (1) (2011) 52–59. doi:10.1016/j.jmr.2011.04.003.

[97] I. Noda, Frontiers of Two-Dimensional Correlation Spectroscopy. Part 1. New concepts and noteworthy developments, Journal of Molecular Structure 1069 (2014) 3–22. doi:10.1016/j.molstruc.2014.01.025.

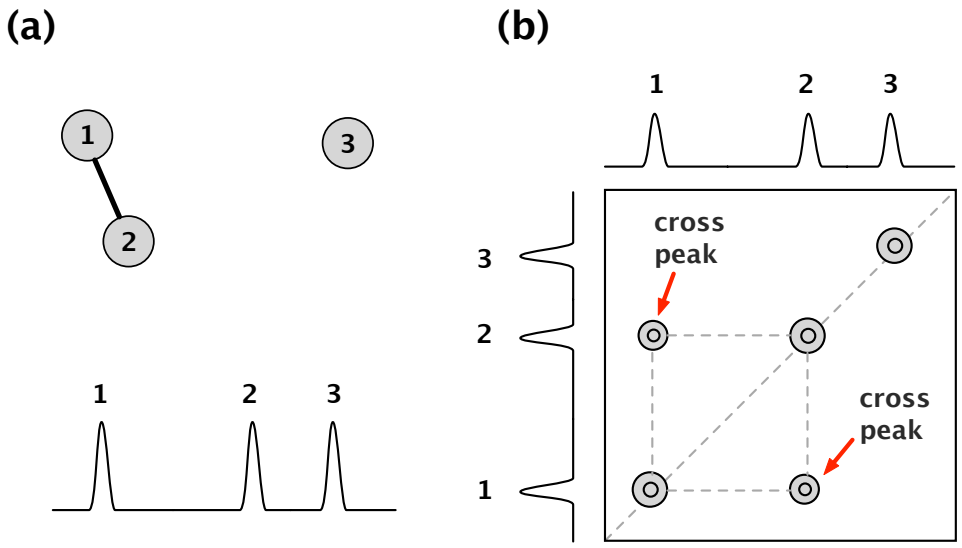

Fig. 1. (a) A schematic drawing of a system of three spins labeled 1, 2, and 3. When spin 1 and spin 2 have correlation while spin 3 is isolated, the cross peak between 1 and 2 appears, as depicted in (b).

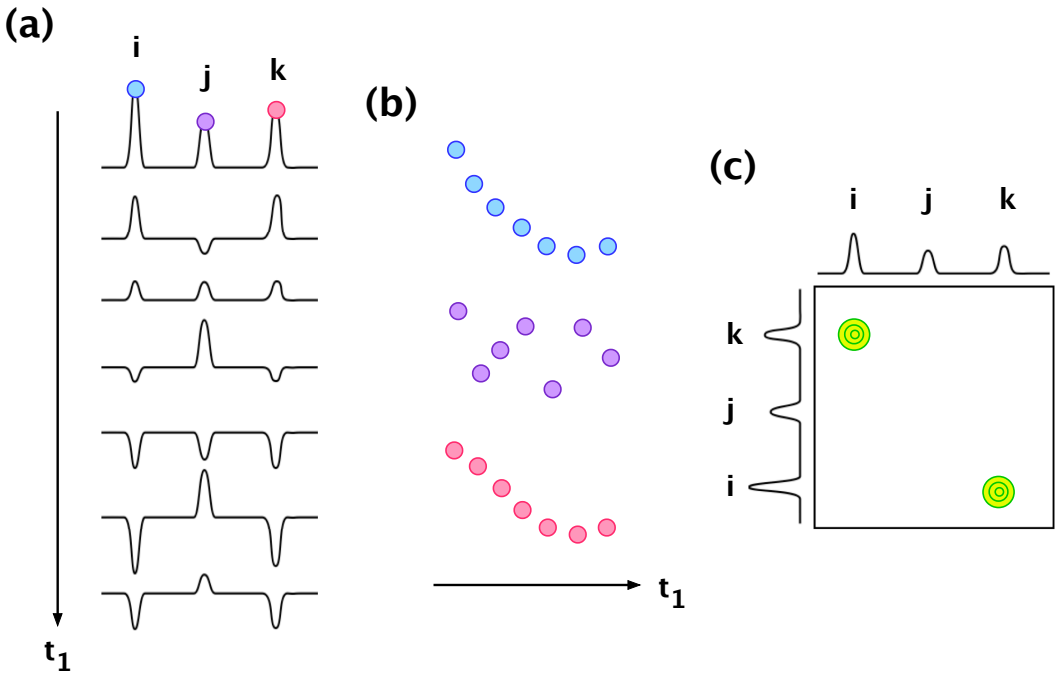

Fig. 2. (a) A schematic drawing of an array of one-dimensional spectra of a homonuclear three spin system with incremented evolution time t_1. We suppose that the magnetizations of the spins labeled with i, j, and k changes with time as depicted in (b). Since the way that the magnetizations of i and k change with t_1 is somewhat correlated, a covariance cross peak appears between i and k, as drawn in (c), whereas the time dependence of the j magnetization is quite different from others, resulting in no appreciable covariance cross peaks.

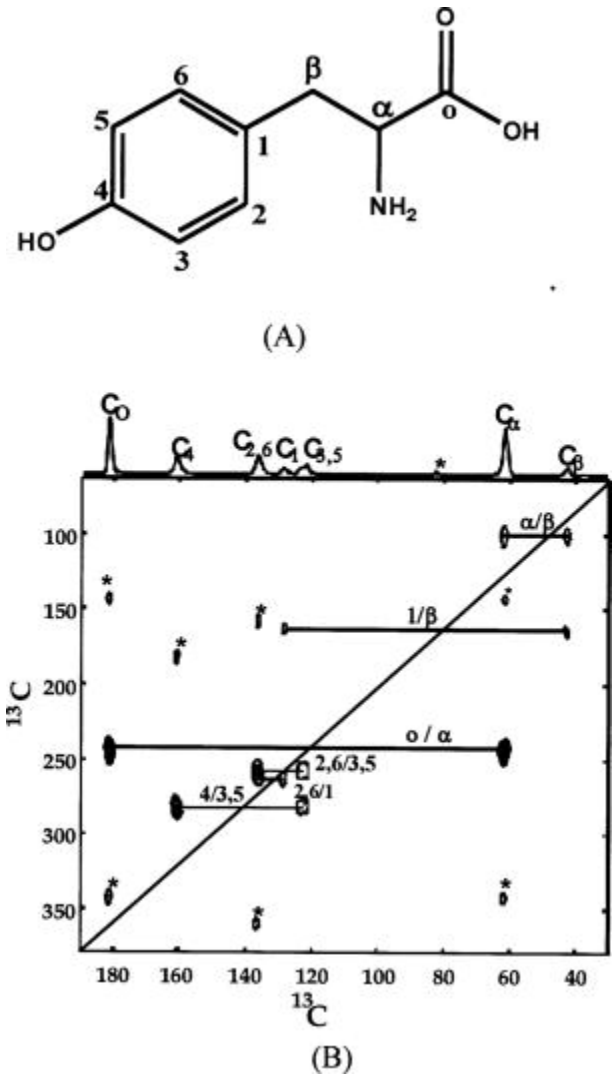

Fig. 3. A ^{13}C double-quantum correlation spectrum (bottom) of ^{13}C-labeled tyrosine (top). 2D-FT was performed on 125 data arrays. This spectrum is to be compared with the covariance spectrum shown in Fig. 4(A), which was obtained using the identical data source. Reprinted with permission from Ref. [74]. Copyright 2008 American Institute of Physics.

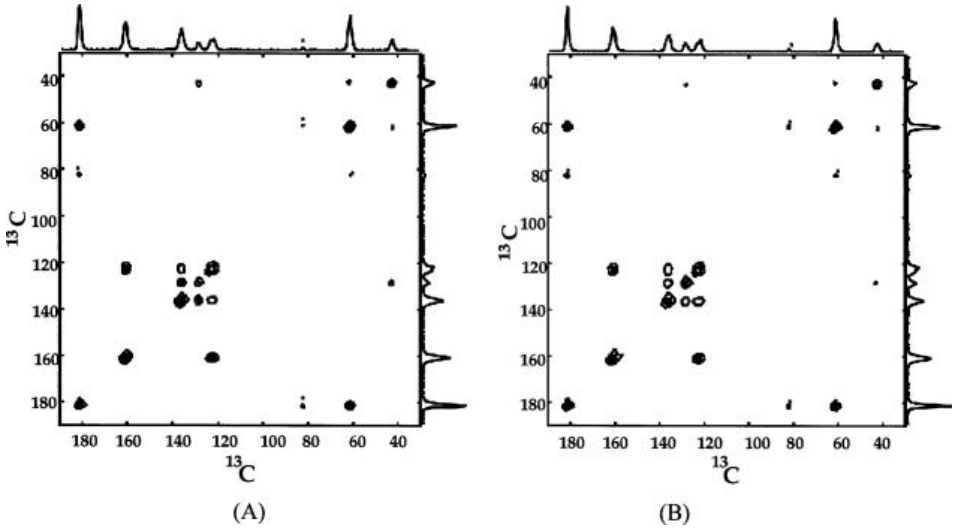

Fig. 4. Covariance ^{13}C double-quantum spectra of ^{13}C-labeled tyrosine obtained from the same data source as that used to obtain the conventional double-quantum spectrum shown in Fig. 3. (A) was obtained from 125 data arrays. Even the array length was intentionally reduced to only 25, the covariance spectrum shows little degredation, as demonstrated in (B). Reprinted with permission from Ref. [74]. Copyright 2008 American Institute of Physics.

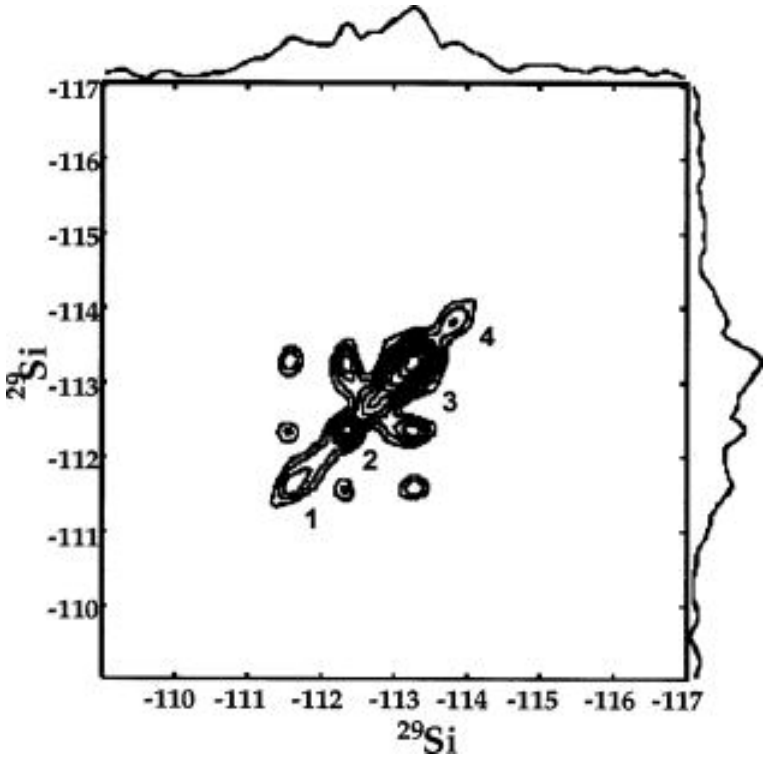

Fig. 5. A ^{29}Si INADEQUATE spectrum of silicate 1. Covariance processing was performed on 32 data arrays. Reprinted with permission from Ref. [74]. Copyright 2008 American Institute of Physics.

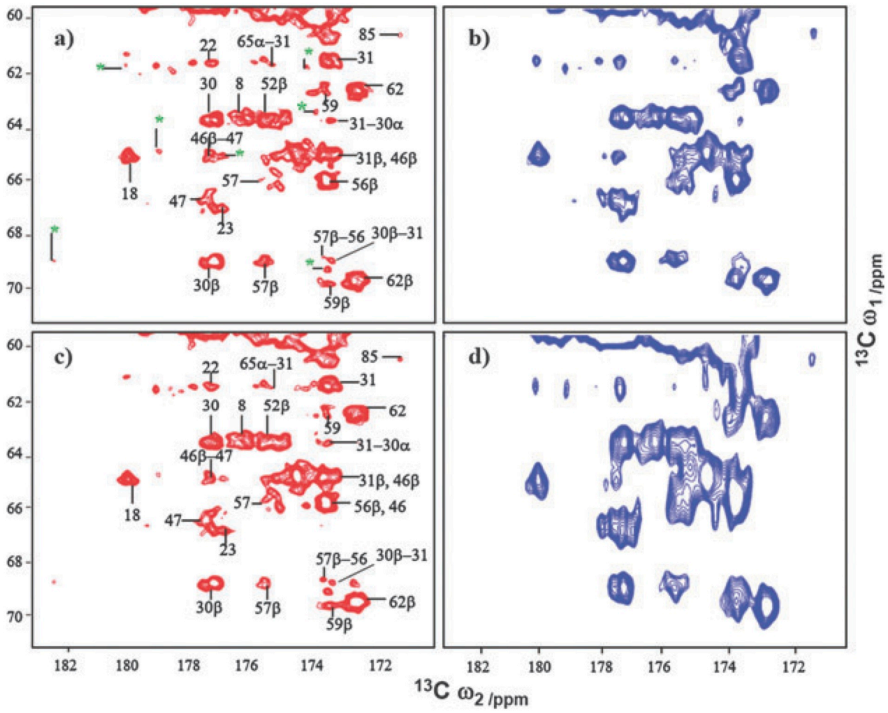

Fig. 6. ^{13}C-^{13}C correlation spectra of a microcrystalline sample of domain-swapped homodimer of catabolite repression phosphocarrier (Crh) protein. A region covering carbonyl-aliphatic correlation is cropped. (a) and (c) represent covariance spectra obtained from 512 and 256 data arrays, respectively. For comparison, the corresponding 2D-FT spectra are shown in (b) and (d), where the degradation of the spectral resolution is appreciable. Reproduced from Ref. [75] with permission of the Royal Society of Chemistry.

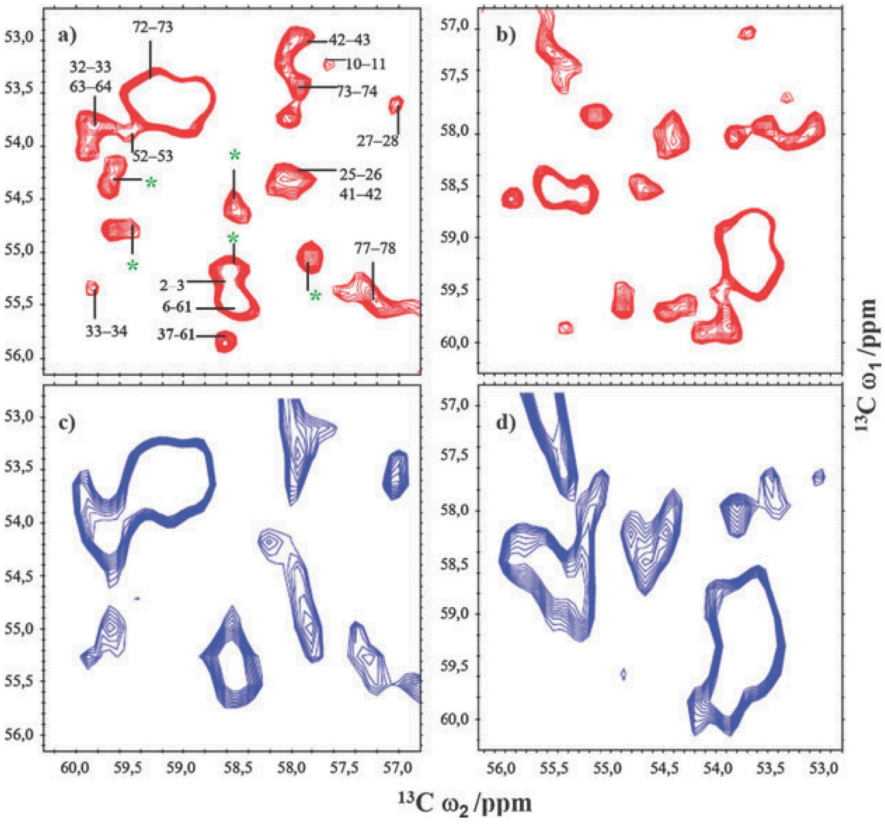

Fig. 7. ^{13}C-^{13}C correlation spectra of a microcrystalline sample of domain-swapped homodimer of catabolite repression phosphocarrier (Crh) protein. A region covering aliphatic-aliphatic correlation is cropped. (a) and (b) are covariance spectra, while (c) and (d) shows 2D-FT spectra obtained from the same data source. Reproduced from Ref. [75] with permission of the Royal Society of Chemistry.

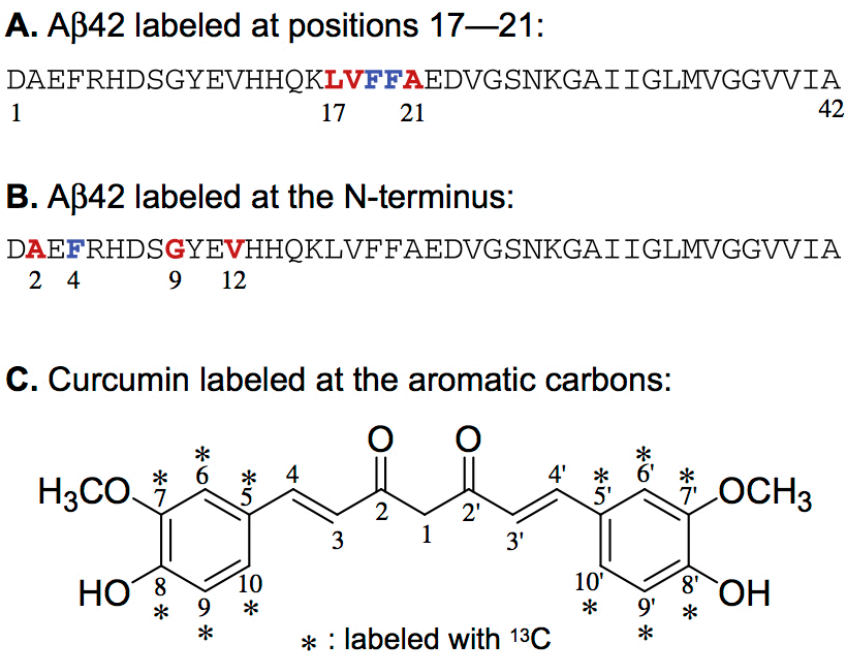

Fig. 8. Amino acid sequence of Aβ42 and a curcumin molecule. Reprinted with permission from Ref. [76]. Copyright 2011 Elsevier.

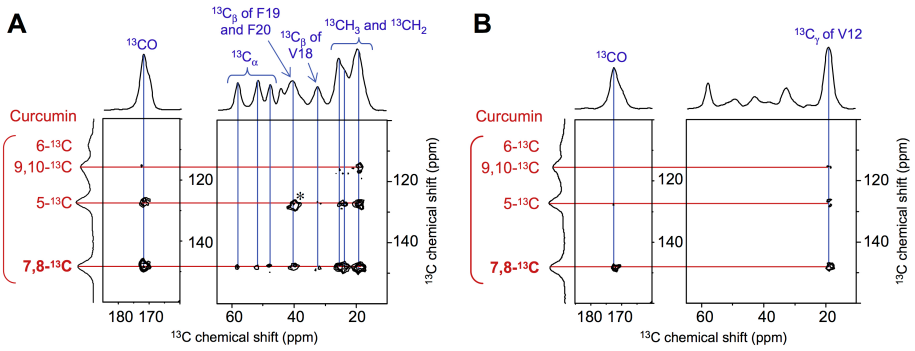

Fig. 9. Covariance-processed ^{13}C correlation spectra obtained in ^{13}C-labeled samples of Aβ42 fibril mixed with curcumin. Reprinted with permission from Ref. [76]. Copyright 2011 Elsevier.

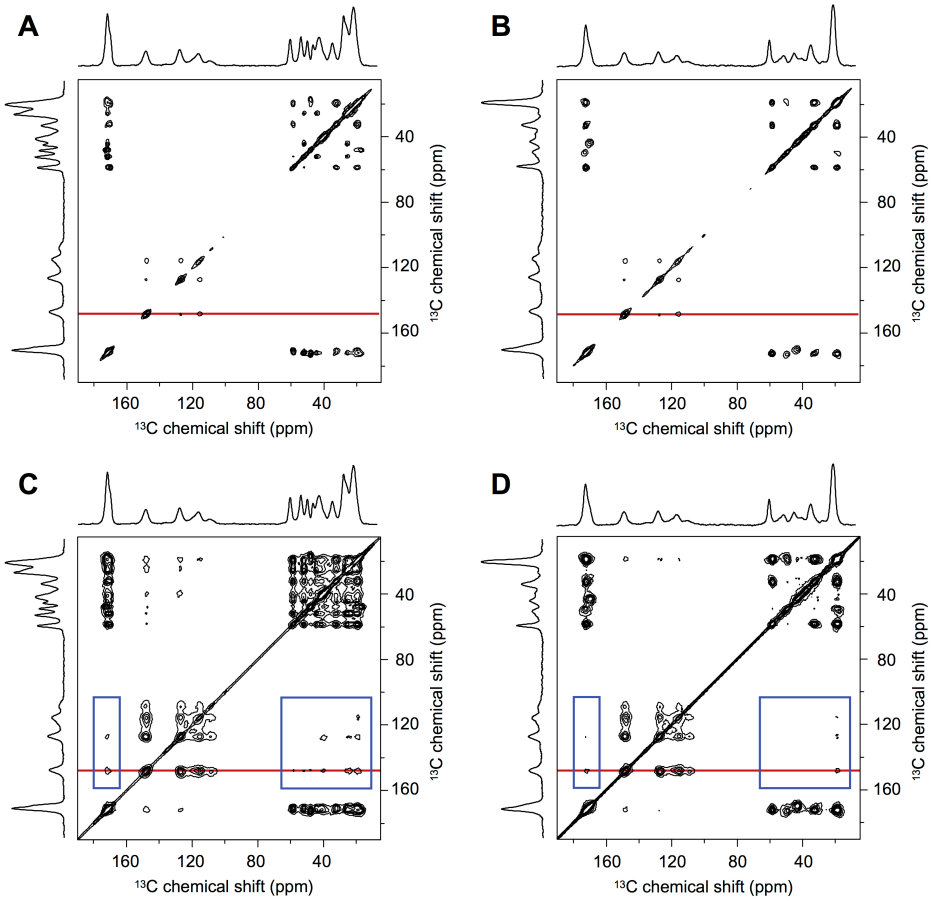

Fig. 10. Mixing-time dependence of ^{13}C covariance spectra in ^{13}C-labeled samples of Aβ42 fibril mixed with curcumin. (a) and (b) were obtained with a mixing time of 50 ms in Aβ42 labeled at the 17-21 residues and at the N-terminus (see Fig. 8). (c) and (d) were obtained with a mixing time of 500 ms. Reprinted with permission from Ref. [76]. Copyright 2011 Elsevier.

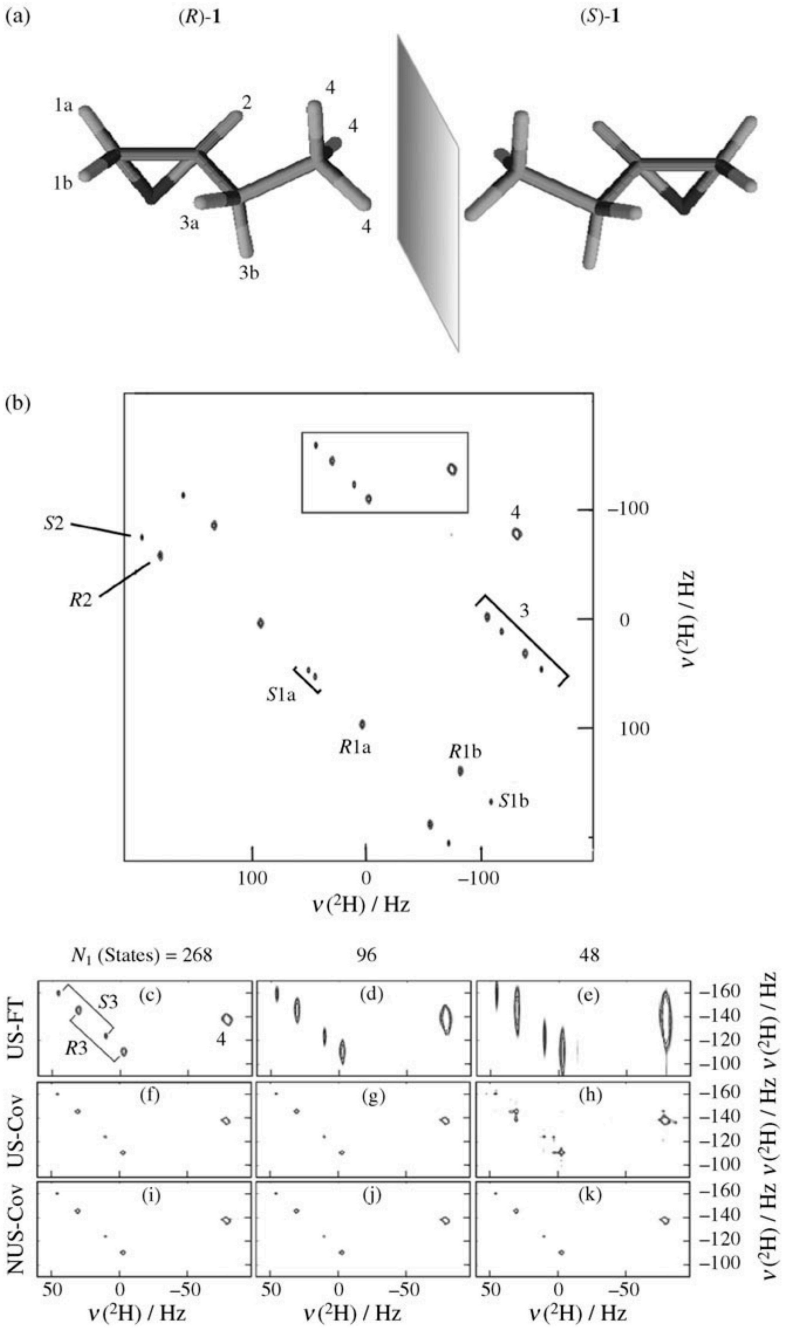

Fig. 11. (a) R and S enantiomers of 2-ethyloxiane. (b) A ^{2}H Q-COSY Fz spectrum of 2-ethyloxirane obtained from a 268 uniformly t_1-incremented data array by the FT method. (c)-(k) Comparison of spectra obtained by FT with uniform sampling, covariance with uniform sampling, and covariance with non-uniform sampling. Reprinted with permission from Ref. [78]. Copyright 2011 John Wiley and Sons.

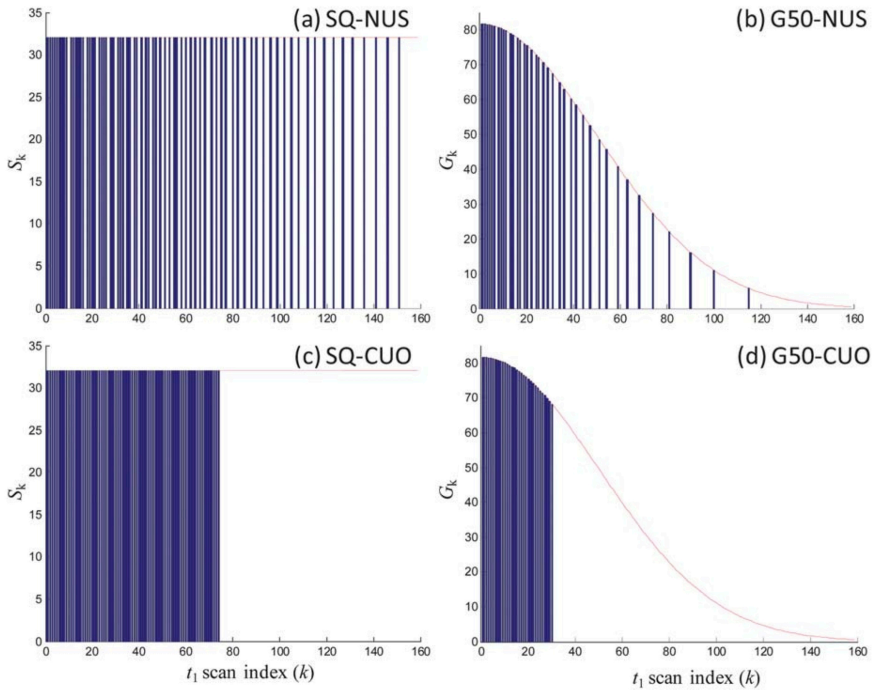

Fig. 12. Four options of signal-accumulation profiles. The positions and the heights of the vertical blue bars represent the timing of the data sampling and the number of accumulations. Reproduced from Ref. [83] with permission of the Royal Society of Chemistry.

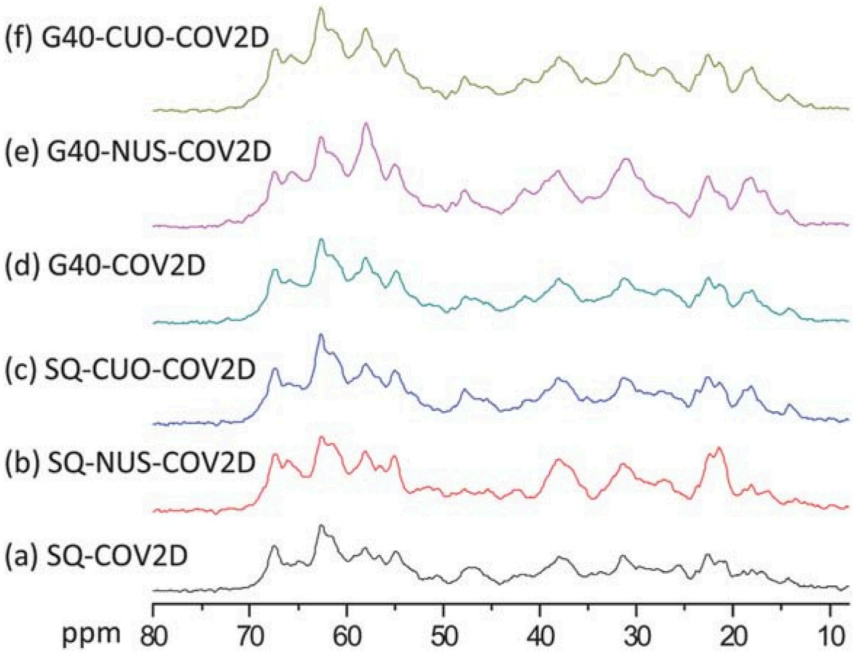

Fig. 13. One-dimensional slice spectra of a 2D covariance spectrum obtained with various accumulation profiles. Reproduced from Ref. [83] with permission of the Royal Society of Chemistry.

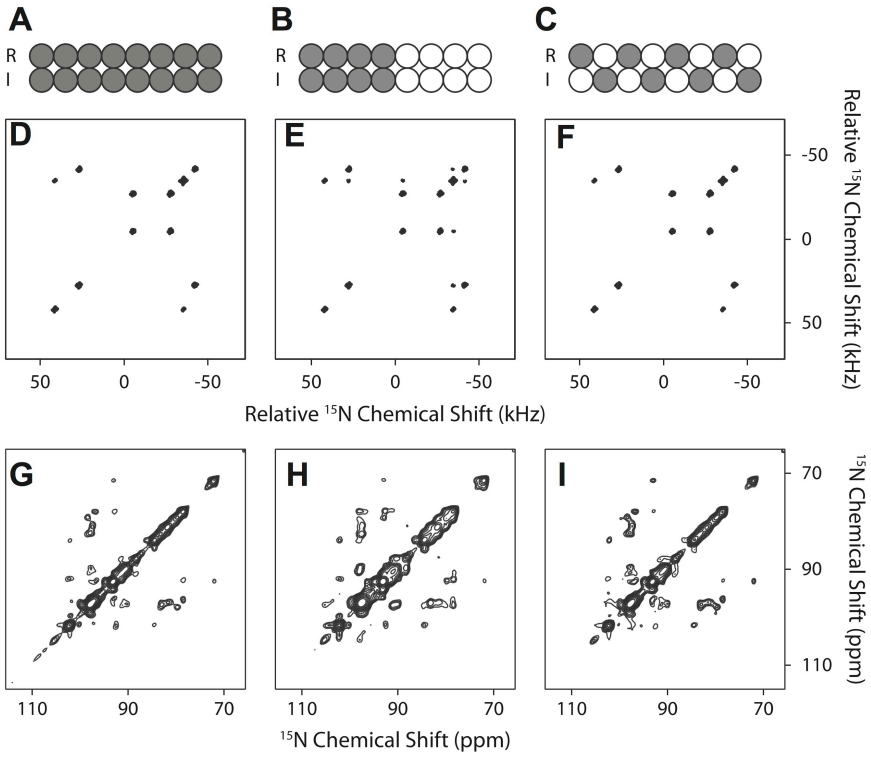

Fig. 14. (a)-(c) Schematic illustrations of (a) conventional sampling, (b) truncated sampling, and (c) alternative States sampling. (d)-(f) simulated spectra generated using (a)-(c) schemes. (g)-(i) Experimental ^{15}N exchange spectra obtained using (a)-(c) schemes. Reprinted with permission from Ref. [79]. Copyright 2014 Elsevier.

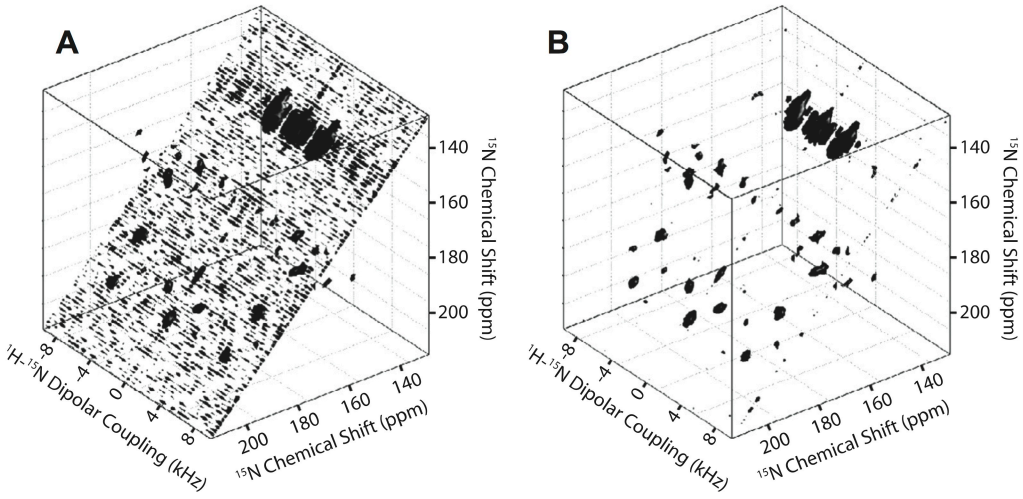

Fig. 15. (a) A three dimensional ^{1}H-^{15}N/^{15}N/^{15}N spectrum. The ^{1}H-^{15}N dipolar–coupling dimension was reconstructed by compressed sensing, while ^{15}N-^{15}N correlation by covariance in combination with alternative States sampling. Reprinted with permission from Ref. [79]. Copyright 2014 Elsevier.

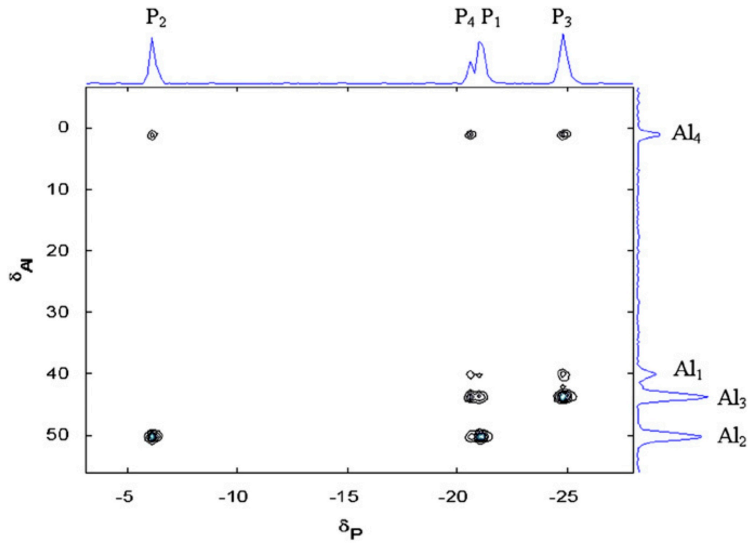

Fig. 16. A source ^{27}Al-^{31}P SPAM-MQ-J-HETCOR spectrum of $AlPO_4$-14, from which ^{27}Al-^{27}Al/^{31}P-^{31}P indirect covariance HOMCOR spectra (Figs. 17-18) were obtained. Reprinted with permission from Ref. [86]. Copyright 2007 Elsevier.

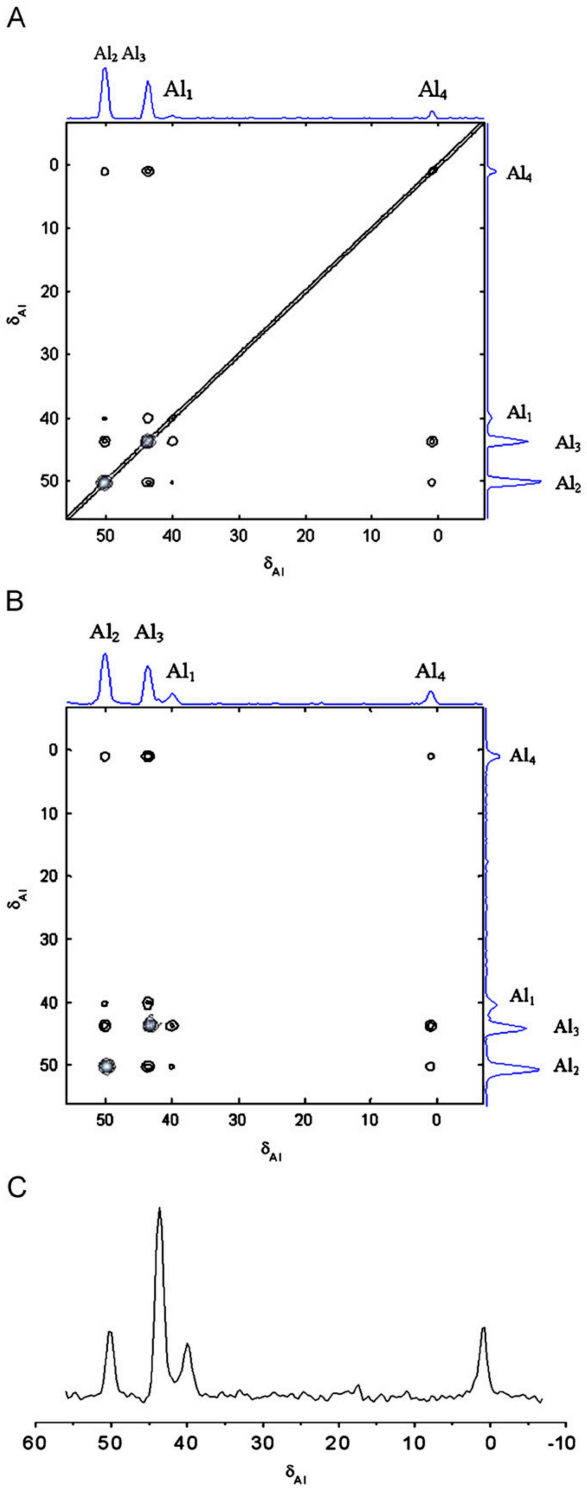

Fig. 17. ^{27}Al-^{27}Al J-coupled indirect covariance spectra obtained from the ^{27}Al-^{31}P SPAM-MQ-J-HETCOR spectrum shown in Fig. 16. Reprinted with permission from Ref. [86]. Copyright 2007 Elsevier.

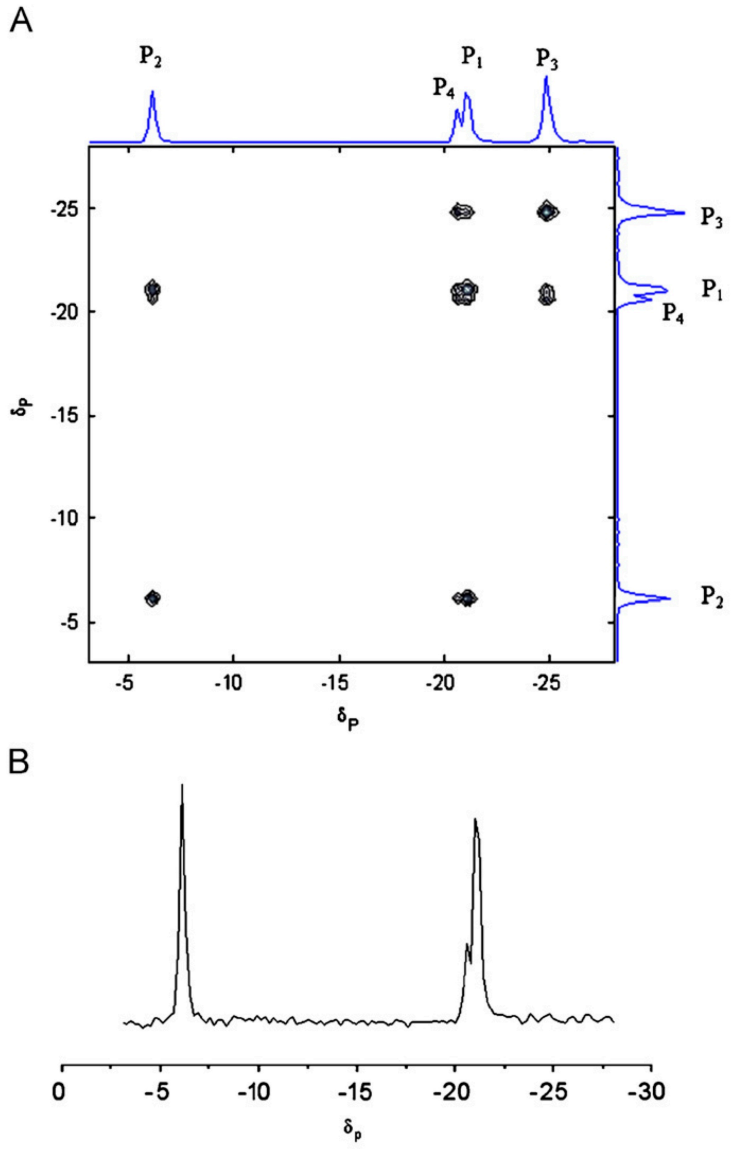

Fig. 18. A ^{31}P-^{31}P J-coupled indirect covariance spectrum obtained from the ^{27}Al-^{31}P SPAM-MQ-J-HETCOR spectrum shown in Fig. 16. Reprinted with permission from Ref. [86]. Copyright 2007 Elsevier.

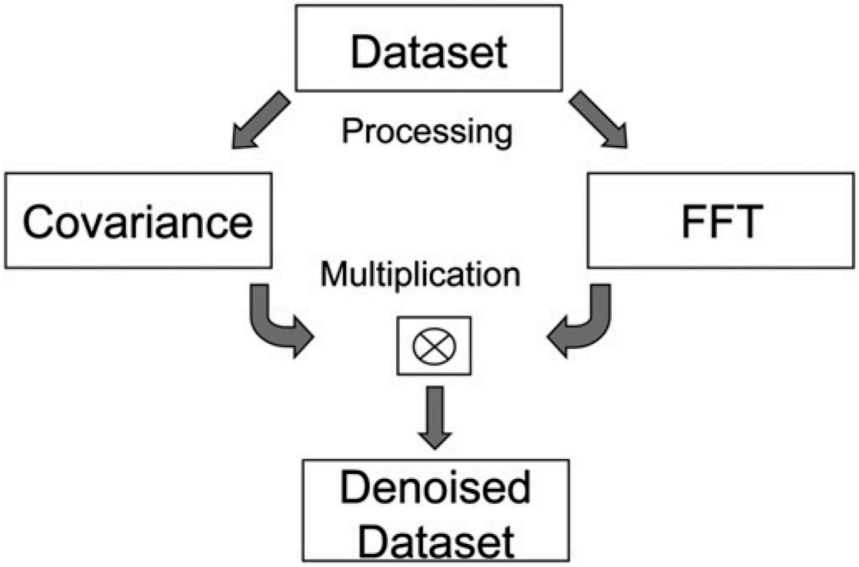

Fig. 19. A diagram describing the flow of the dual transformation denoising (DTD) process. Adopted from ref. [93]. Copyright 2007 Elsevier.

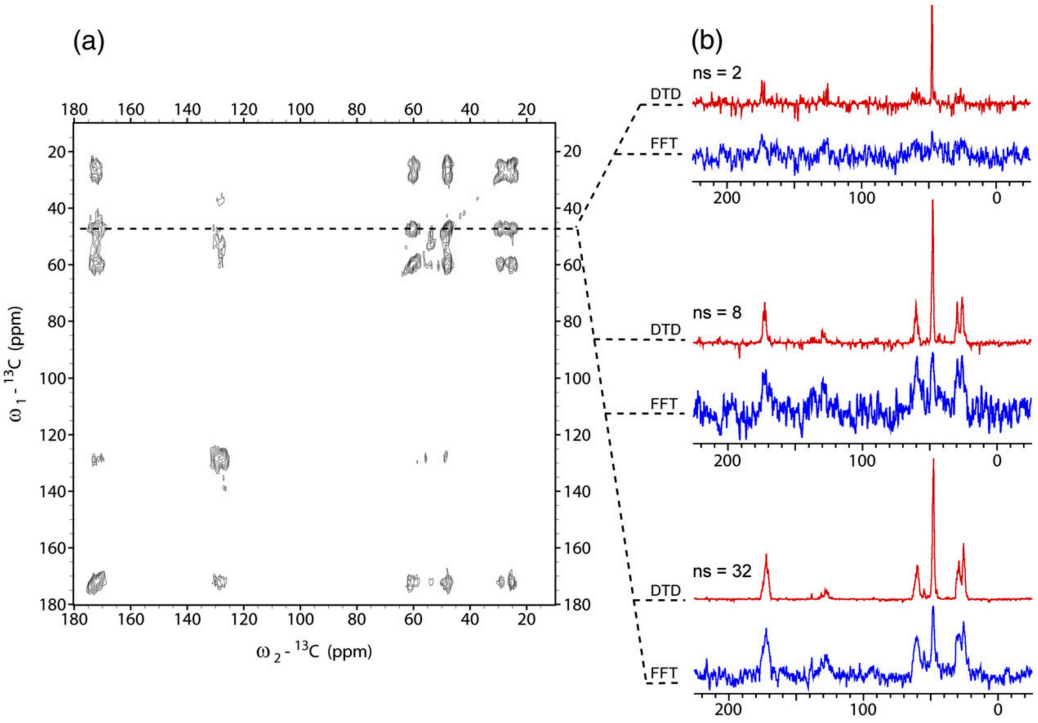

Fig. 20. Comparison of ^{13}C-^{13}C proton-driven spin diffusion spectra obtained using DTD and FFT. Adopted from ref. [93]. Copyright 2007 Elsevier.

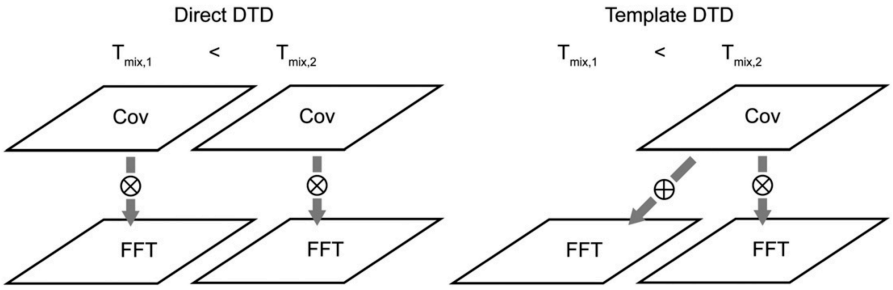

Fig. 21. Schematic diagrams of direct DTD and template DTD. Adopted from ref. [93]. Copyright 2007 Elsevier.

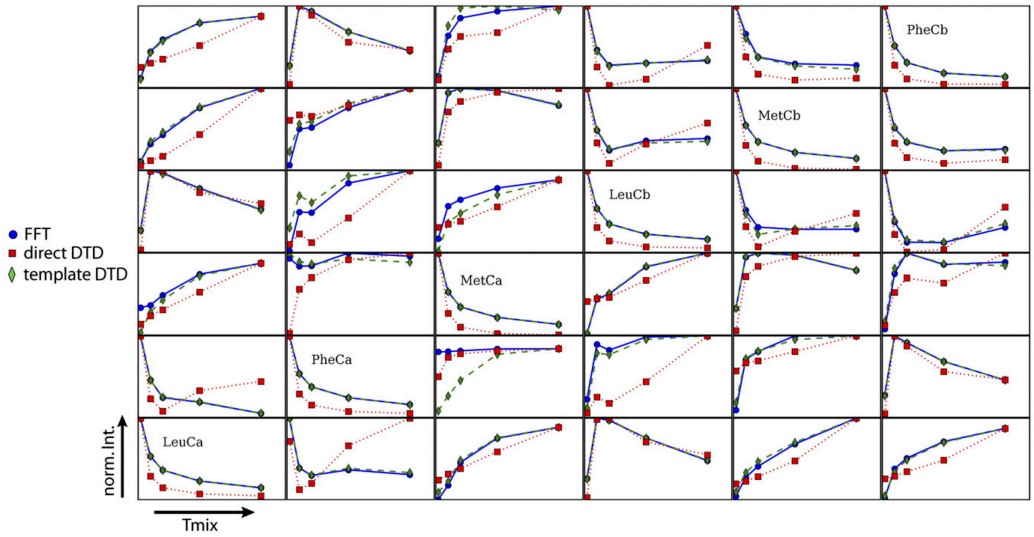

Fig. 22. Experimental buildup curves of ^{13}C-^{13}C cross peaks in FFT, direct DTD, and template DTD spectra obtained in methionine-leucine-phenylalanine tripeptide. Adopted from ref. [93]. Copyright 2007 Elsevier.

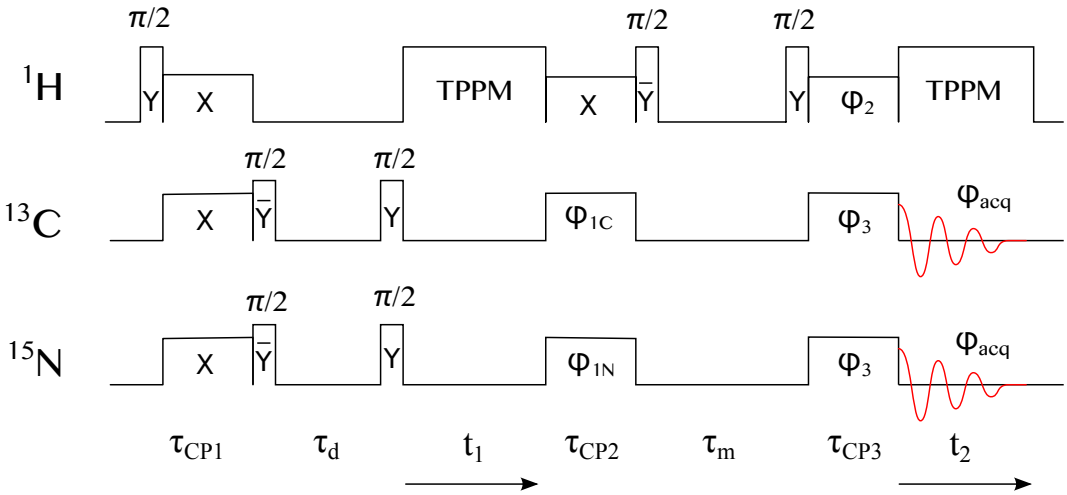

Fig. 23. A pulse sequence of ^{1}H-^{1}H dipolar-coupling mediated ^{13}C/^{15}N chemical shift correlation experiments used to obtain homo- and heteronuclear covariance spectrum. Reproduced from ref. [94] with permission from the PCCP Owner Societies.

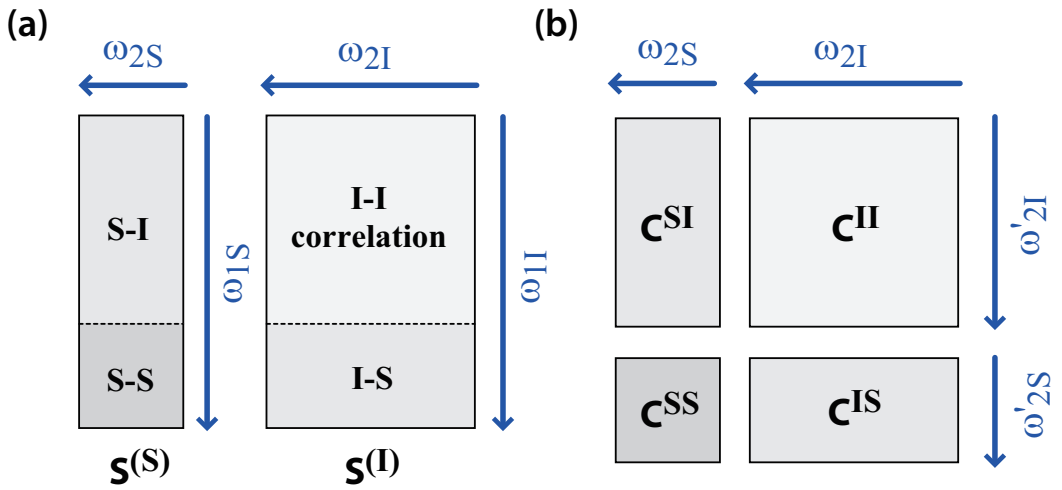

Fig. 24. Correspondence between the conventional 2D FT and homo- and heteronuclear covariance spectra. Reproduced from ref. [94] with permission from the PCCP Owner Societies.

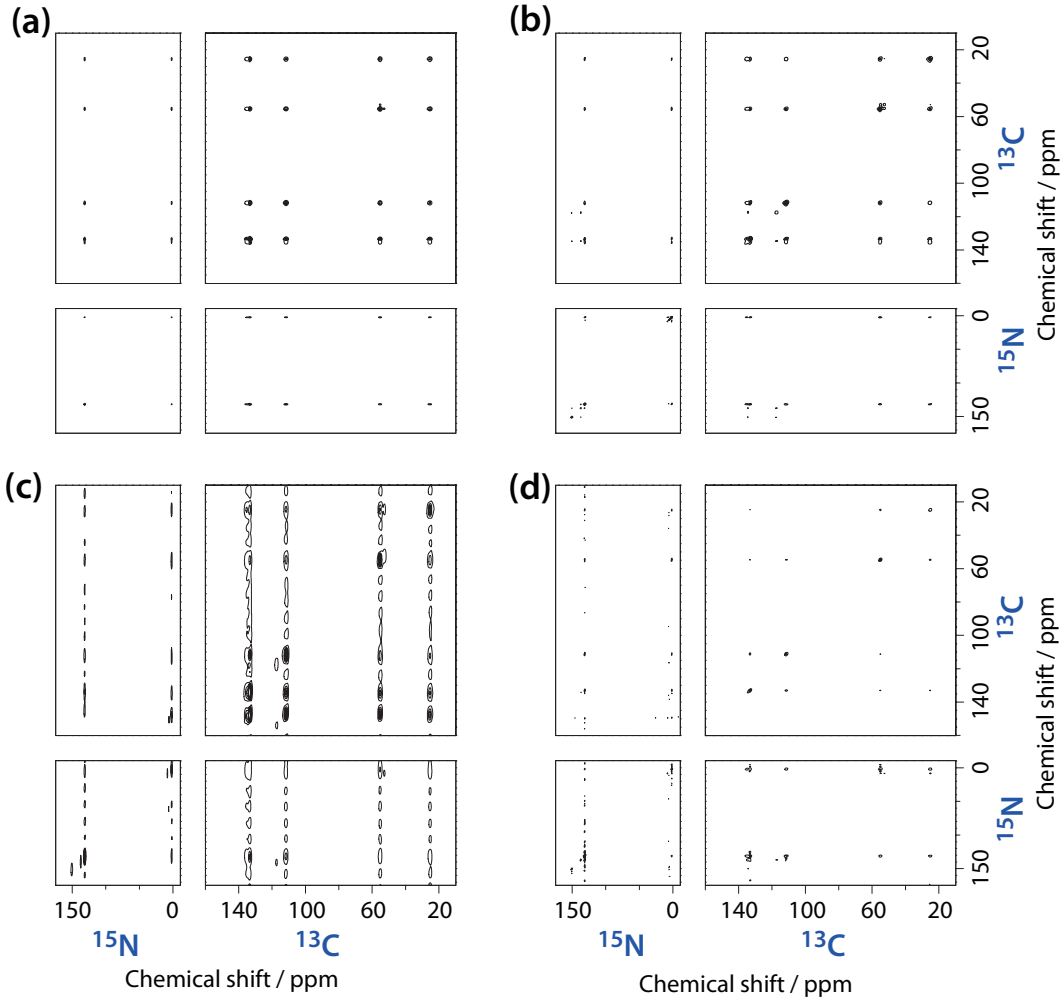

Fig. 25. (a) 2D covariance spectra of ^{1}H-^{1}H dipolar coupling mediated ^{13}C/^{15}N chemical shift correlation experiment obtained in uniformly ^{13}C, ^{15}N-labeled histidine with the pulse sequence described in Fig. 23. The number of t_1 increments was 32. (b) The square root of the 2D covariance spectrum in (a). (c) A 2D FT spectrum obtained from the identical data set as that used to obtain the covariance spectra in (a) and (b). (d) A 2D FT spectrum obtained with 256 t_1 increments. Reproduced from ref. [94] with permission from the PCCP Owner Societies.

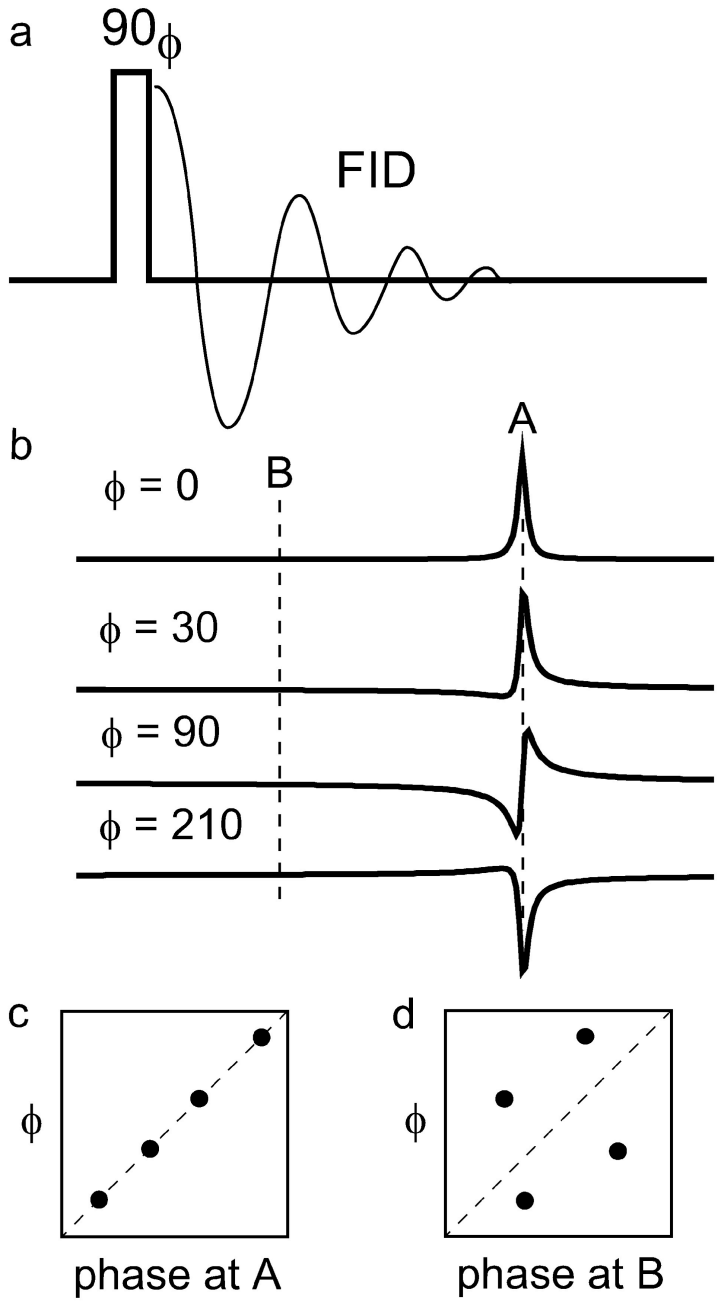

Fig. 26. Schematic illustrations of correlation between the phases of rf pulses and of the individual complex data points of NMR spectra. Reproduced from ref. [95] with permission of the PCCP Owner Societies.

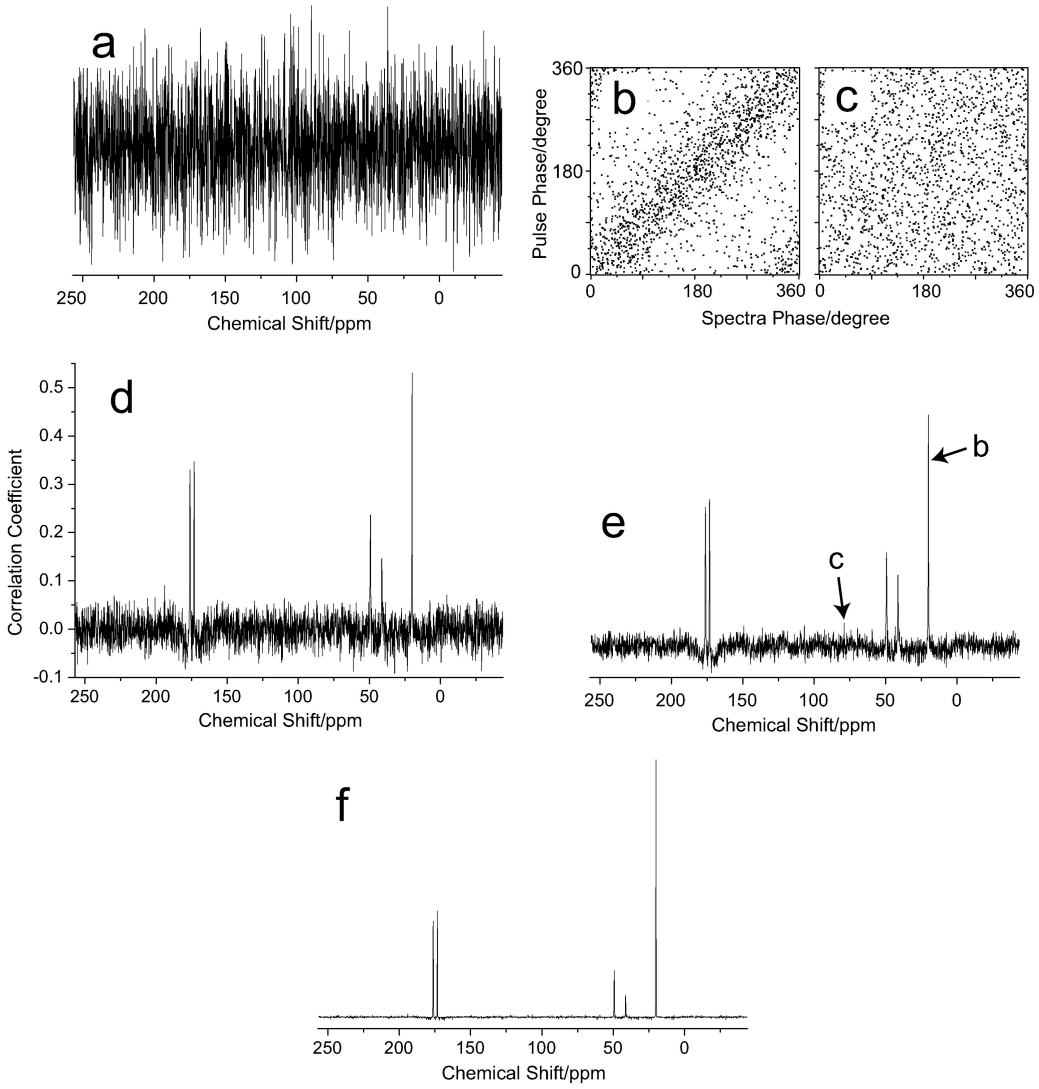

Fig. 27. A demonstration of phase covariance. (a) A ^{13}C CPMAS spectrum of a low-concentration mixture of glycine and L-alanine in KBr powder obtained from a single FID with no accumulation. (b)(c) Phase distributions of 1800 data points at the methyl peak position and an arbitrary spectral position with no signal. (d) A normalized covariance spectrum. (e) A conventional averaged spectrum obtained with phase correction followed by summation. (f) A phase-covariance weighted spectrum obtained by multiplying the spectra shown in (d) and (e). Reproduced from ref. [95] with permission of the PCCP Owner Societies.

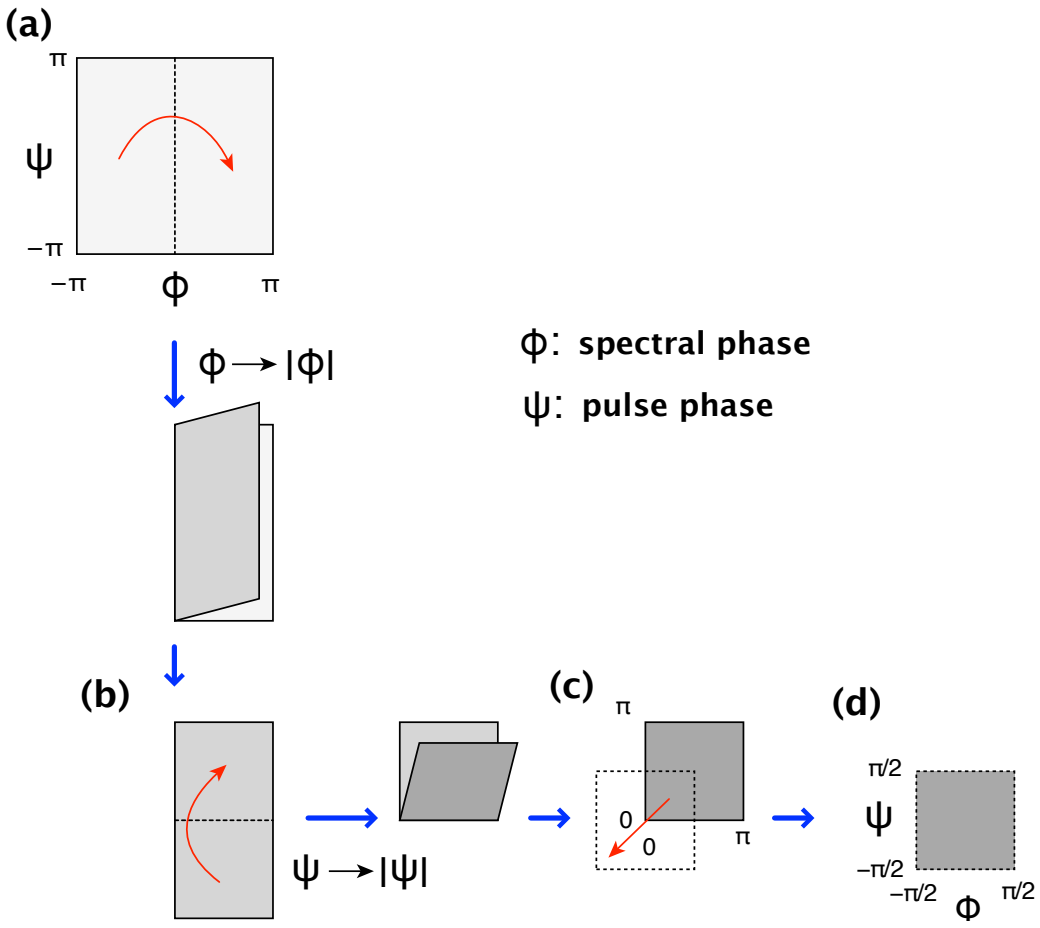

Fig. 28. A geometric account for the transformation of the phase-distribution map proposed in ref. [96].